

# Controlling emergent dynamical behavior via phase-engineered strong symmetries

Marc Nairn, Beatriz Olmos, and Parvinder Solanki

*Institut für Theoretische Physik, Universität Tübingen,  
Auf der Morgenstelle 14, 72076 Tübingen, Germany*

(Dated: February 24, 2026)

Symmetry constraints provide a powerful means to control the dynamics of open quantum systems. However, the set of accessible control parameters is often limited. Here, we show that a tunable phase in the collective light-matter coupling of a cavity QED system induces a phase-dependent strong symmetry of the Liouvillian, enabling dynamical control of the open quantum system evolution. We demonstrate that tuning this phase substantially reduces the critical driving strength for dissipative phase transitions between stationary and non-stationary phases. We illustrate this mechanism in two experimentally relevant cavity QED settings: a two-species ensemble of two-level atoms and a single-species ensemble of three-level atoms. Our results establish phase control as a versatile tool for engineering dissipative phase transitions, with implications for quantum state preparation.

*Introduction.*— Symmetries play a central role in modern physics by constraining dynamics, enforcing conservation laws, and shaping phases of matter and their transitions [1, 2]. In open quantum systems [3, 4], where coherent and dissipative processes coexist, symmetries impose stringent constraints on both the structure of the dynamics and the stationary and non-stationary states that they support [5, 6]. In these systems, when present, so-called strong symmetries remain preserved under both coherent evolution and dissipation, enforcing microscopic conservation laws in contrast to the ensemble-averaged conservation laws associated with weak symmetries [7]. Such symmetries can give rise to decoherence-free subspaces [8–14] and enable rich non-equilibrium phenomena, including non-stationary phases [15–18] with applications in sensing [19, 20], heat engines [21, 22], and energy storage [23].

A complementary route to controlling open-system dynamics exploits phase-engineered interference, achievable through geometric design [24] or reservoir engineering [25]. Such phases can be global, generating collective nonlinear effects protected by symmetries [26], or appear as non-gaugeable relative phases that enable non-reciprocal behavior [27–29]. These mechanisms underpin applications ranging from directional amplification [30–32] to the emergence of novel dynamical phases [33–36]. Despite these advances, the use of phase-dependent symmetries themselves as a resource for controlling open-system dynamics has remained largely unexplored.

In this work, we show that the interplay between strong symmetries and tunable phases provides a powerful and systematic route to controlling dynamical phenomena in collective light-matter systems. We consider a driven-dissipative cavity QED platform that exhibits dissipative phase transitions between stationary and non-stationary states, also known as continuous-time crystals [15, 23, 37–

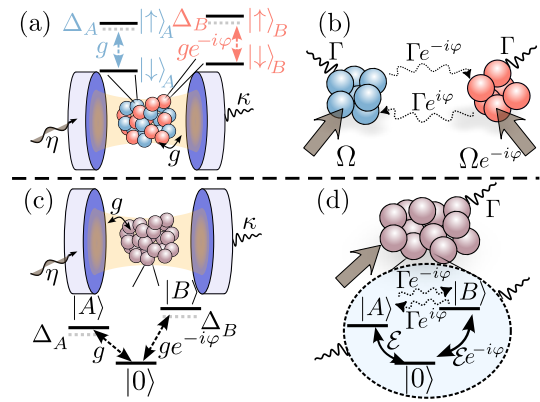


FIG. 1. **Schematic of the setups.** (a) Two species of two-level atoms confined in a single-mode optical cavity with phase-dependent couplings  $g_A = g, g_B = ge^{-i\varphi}$  and (b) description of the effective spin interactions mediated by the cavity. (c) Atomic gas where each atom is modeled as a three-level system with state-dependent couplings  $g_A = g, g_B = ge^{-i\varphi}$  and (d) effective atom-only description.

55]. We demonstrate that a tunable phase in the collective light-matter coupling induces a phase-dependent strong symmetry that reshapes the onset and character of the non-stationary dynamics, enabling access to time-crystalline regimes at substantially reduced driving strengths. We establish the generality of this mechanism by analyzing two variants of the Tavis-Cummings model: a two-species ensemble of two-level atoms and a single-species three-level atomic gas in a single-mode cavity. Our results identify phase-controlled strong symmetries as a versatile tool for engineering non-stationary phases and controlling dissipative phase transitions in open quantum systems, with potential applications in quantum state preparation.

*Strong symmetries in open quantum systems.*— Within the Born-Markov approximation, the time evolution of the density matrix  $\hat{\rho}$  of an open quantum system is governed by the Gorini-Kossakowski-

Sudarshan-Lindblad master equation (GKSL),

$$\dot{\hat{\rho}} = \mathcal{L}(\hat{\rho}) \equiv -\frac{i}{\hbar}[\hat{H}, \hat{\rho}] + \sum_k \mathcal{D}[\hat{L}_k]\hat{\rho}, \quad (1)$$

where  $\hat{H}$  is the Hamiltonian,  $\hat{L}_k$  are the Lindblad jump operators,  $\mathcal{D}[\hat{L}_k]\hat{\rho} = \hat{L}_k\hat{\rho}\hat{L}_k^\dagger - \{\hat{L}_k^\dagger\hat{L}_k, \hat{\rho}\}/2$  denotes the dissipator and  $\mathcal{L}$  is the Liouvillian superoperator.

A system exhibits a *strong symmetry* if there exists an operator  $\hat{A}$  that commutes with both the Hamiltonian and all Lindblad jump operators, i.e.,  $[\hat{A}, \hat{H}] = 0$  and  $[\hat{A}, \hat{L}_k] = 0 \forall k$  [5–7]. This dual commutation relation partitions the Hilbert space into invariant symmetry sectors,  $\mathcal{H} = \bigoplus_\lambda \mathcal{H}_\lambda$ , corresponding to the eigenspaces of  $\hat{A}$ . As a result, the dynamics generated by  $\mathcal{L}$  is decoupled across sectors. Decomposing the initial state as  $\hat{\rho}(0) = \sum_{\lambda, \lambda'} \hat{\rho}_{\lambda\lambda'}(0)$  with  $\hat{\rho}_{\lambda\lambda'}(0) = \hat{\Pi}_\lambda \hat{\rho}(0) \hat{\Pi}_{\lambda'}$  and  $\hat{\Pi}_\lambda$  being the projector onto  $\mathcal{H}_\lambda$ , the coherences between different symmetry sectors ( $\lambda \neq \lambda'$ ) do not contribute to the long-time dynamics [45]. Consequently, the steady state of Eq. (1) assumes the block-diagonal form

$$\hat{\rho}^{\text{ss}} = \lim_{t \rightarrow \infty} e^{\mathcal{L}t} \hat{\rho}(0) = \sum_\lambda w_\lambda \hat{\rho}_\lambda^{\text{ss}}, \quad (2)$$

where the conserved sector weights (or overlaps)  $w_\lambda = \text{Tr}[\hat{\Pi}_\lambda \hat{\rho}(0)]$  are fixed by the initial state.

In the following, we show that in collective cavity QED systems, a tunable phase in the light–matter coupling modifies the underlying strong symmetry, thereby reshaping the dynamical constraints imposed by Eq. (1) and controlling the onset of dissipative phase transitions.

*Two-species model.*— We first consider an ensemble of  $N$  atoms interacting with a single-mode driven cavity. The atoms belong to two different species,  $A$  and  $B$ , each comprising  $N/2$  two-level atoms with states  $|\downarrow\rangle_{A/B}$  and  $|\uparrow\rangle_{A/B}$  [see Fig. 1(a)]. Each species couples collectively to the cavity field with coupling strength  $g_{A/B}$  and atomic detuning  $\Delta_{A/B}$ . As detailed in the Supplemental Material (SM) [56], both the magnitude and phase of the couplings, as well as the detunings, can be controlled experimentally using external Raman lasers. In the following, we focus on the situation in which the two species differ only by a controllable phase  $\varphi$ , i.e.  $g_A = g$ ,  $g_B = ge^{-i\varphi}$ , and  $\Delta = \Delta_A = \Delta_B$ .

In an appropriate rotating frame, the system dynamics is governed by the Hamiltonian  $\hat{H}_{2L} = \hat{H}_{\text{cav}} + \hat{H}_{\text{int}} + \hat{H}_{\text{at}}$  (see SM [56] for details of the derivation). The cavity contribution reads  $\hat{H}_{\text{cav}} = \hbar\Delta_c \hat{a}^\dagger \hat{a} + i\hbar\eta\sqrt{N}(\hat{a}^\dagger - \hat{a})$ , where  $\hat{a}$  ( $\hat{a}^\dagger$ ) annihilates (creates) a cavity photon,  $\eta$  is the driving rate, and  $\Delta_c$  the cavity detuning. Throughout this work we set  $\Delta_c = 0$ ; qualitatively similar be-

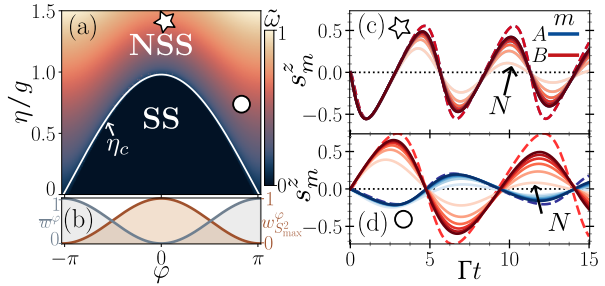


FIG. 2. **Phase enabled nonstationary states.** (a) Mean-field phase diagram showcasing the effect of tunable phase  $\varphi$  on the transition between stationary (SS) and nonstationary states (NSS), and (b) the corresponding weight distribution in the Dicke subspace,  $w_{S^{\varphi}}^{\varphi}$  and its complement  $\bar{w}^{\varphi}$ . Finite-size dynamics for highlighted points in (a) illustrating the usual time-crystalline behavior and the lowering of the threshold value, panels (c) and (d), respectively. We consider system sizes  $N \in (10, 20, \dots, 60)$  (lines with increasing color intensity). The results are benchmarked against the mean-field values (dashed) with  $g/\kappa = 0.1$  and  $\Delta = 0$ .

havior persists for  $\Delta_c \neq 0$  (see SM [56]). The atom-cavity interaction is  $\hat{H}_{\text{int}} = \hbar g/\sqrt{N}(\hat{a}^\dagger \hat{S}_\varphi + \hat{a} \hat{S}_\varphi^\dagger)$ , where the phase-dependent spin operator  $\hat{S}_\varphi = \sum_{j=1}^{N/2} (\hat{\sigma}_{jA} + e^{-i\varphi} \hat{\sigma}_{jB})$  encodes the relative phase between the two species, with  $\hat{\sigma}_{jm} = |\downarrow\rangle_{jm}\langle\uparrow|$ . The free atomic Hamiltonian is given by  $\hat{H}_{\text{at}} = \hbar\Delta \hat{S}_\varphi^z$ , with  $\hat{S}_\varphi^z = \frac{1}{2}(\hat{S}_\varphi^\dagger \hat{S}_\varphi - \hat{S}_\varphi \hat{S}_\varphi^\dagger)$ . Photon losses are described by a Lindblad term with decay rate  $\kappa$ . All terms are scaled with  $N$  to ensure a well-defined thermodynamic limit ( $N \rightarrow \infty$ ).

To understand the role of the phase  $\varphi$ , we first analyze the mean-field dynamics in terms of the cavity field  $\alpha = \langle \hat{a} \rangle$  and the rescaled collective spin components  $s_{A/B}^\mu = \langle \hat{S}_{A/B}^\mu \rangle / (N/2)$  with  $\hat{S}_m^\mu = \frac{1}{2} \sum_{j=1}^{N/2} \hat{\sigma}_{jm}^\mu$  and  $\hat{\sigma}_{jm}^{\mu=x,y,z}$  the Pauli matrices for  $m \in \{A, B\}$ . To distinguish stationary from non-stationary phases, we introduce the dominant frequency  $\tilde{\omega}$  extracted from the spectrum of the spin polarization  $\mathcal{F}_{A/B}(\omega) = \int_{-\infty}^{\infty} s_{A/B}^z(t) e^{-i\omega t} dt$ . In all cases considered, the two species oscillate synchronously, so that  $\tilde{\omega} \equiv \tilde{\omega}_A = \tilde{\omega}_B$ .

For  $\varphi = 0$  and  $\Delta = 0$ , the system undergoes a transition from a stationary state ( $\tilde{\omega} = 0$ ) to a non-stationary state ( $\tilde{\omega} > 0$ ) at a critical driving strength  $\eta_c = g$ , as shown in [Fig. 2](a). In contrast, for finite  $\varphi$  the critical driving strength becomes phase-dependent for any initial state with  $|s_{A/B}^z| < 1$ . This behavior is illustrated in [Fig. 2(a)] for the initial state condition  $(\alpha, s_{A/B}^x, s_{A/B}^y, s_{A/B}^z) = (0, 1, 0, 0)$ . Remarkably, the threshold for the onset of non-stationarity is progressively reduced with increasing  $|\varphi|$  and vanishes in the limit  $\varphi \rightarrow \pm\pi$ .

In the following section, we show that this phase-

enabled reduction of the critical drive originates from a modification of an underlying strong symmetry, which reshapes the accessible dynamical sectors of the system.

*Symmetries and dynamical phases in the two-species model.*— In the limit of strong dissipation  $\kappa \gg g, \eta, \Delta$ , the cavity field can be adiabatically eliminated, yielding an effective spin-only description (see SM [56]), [Fig. 1(b)]. The reduced spin density matrix  $\hat{\mu}_s$  then evolves according to

$$\dot{\hat{\mu}}_s = -\frac{i}{\hbar}[\hat{H}_S, \hat{\mu}_s] + \frac{\Gamma}{2S}\mathcal{D}[\hat{S}_\varphi]\hat{\mu}_s, \quad (3)$$

where  $S = N/2$ ,  $\Gamma = 4g^2/\kappa$ , and the effective Hamiltonian reads  $\hat{H}_S = \hbar\Delta\hat{S}_\varphi^z + \hbar\Omega(\hat{S}_\varphi + \hat{S}_\varphi^\dagger)$  with  $\Omega = 2\eta g/\kappa$ . For  $\Delta = 0$  and  $\varphi = 0$ , Eq. (3) reduces to the boundary time crystal (BTC) model [15], which undergoes a transition from a stationary to a time crystalline phase at  $\Omega/(\Gamma/2) = 1$ . This directly accounts for the critical driving strength  $\eta_c = g$  observed in the full cavity-spin model and motivates our identification of the non-stationary phase as a continuous time crystal.

To elucidate the role of the phase  $\varphi$ , we analyze the symmetries of the spin-only dynamics. The operators  $\hat{S}_\varphi, \hat{S}_\varphi^\dagger, \hat{S}_\varphi^z$  generate an  $\mathfrak{su}(2)$  algebra. The associated Casimir operator  $\hat{S}_\varphi^2 = \frac{1}{2}(\hat{S}_\varphi\hat{S}_\varphi^\dagger + \hat{S}_\varphi^\dagger\hat{S}_\varphi) + (\hat{S}_\varphi^z)^2$  commutes with both the Hamiltonian  $\hat{H}_S$  and the jump operators  $\hat{S}_\varphi$ , and therefore constitutes a strong symmetry of the Liouvillian. This symmetry generalizes a total spin conservation in the  $\varphi = 0$  case to a phase-dependent setting. As a consequence, the dynamics decomposes into invariant sectors labeled by the eigenvalues  $S_\varphi^2$  of  $\hat{S}_\varphi^2$ . The system can be thus described in a generalized, phase-dependent Dicke basis. For  $\varphi = 0$ , these sectors coincide with the standard Dicke manifolds; for  $\varphi \neq 0$ , they correspond to rotated collective modes encoding the relative phase between the two subensembles. The weight of each sector is  $w_{S_\varphi^2}^\varphi = \text{Tr}[\hat{\Pi}_{S_\varphi^2}^\varphi \hat{\mu}_s]$ , where  $\hat{\Pi}_{S_\varphi^2}^\varphi$  projects onto the corresponding eigenspace. In practice, the dynamics is governed by the competition between the fully symmetric sector,  $w_{S_\varphi^2}^\varphi = w_{S_\varphi^2}^{\varphi=0}$ , and its complement,  $\bar{w}^\varphi = 1 - w_{S_\varphi^2}^\varphi$ , which collects all contributions outside the permutationally invariant Dicke manifold.

We now connect this symmetry structure to the dynamical phase diagram shown in [Fig. 2(a)]. We consider the initial product state  $\hat{\mu}_s(0) = \bigotimes_{m=A,B} \bigotimes_{j=1}^{N/2} |+\rangle\langle +|_{jm}$  with  $|+\rangle = (|\uparrow\rangle + |\downarrow\rangle)/\sqrt{2}$ , which corresponds to the mean-field condition used in [Fig. 2(a)]. While this choice is not unique, it is particularly instructive because its decomposition into symmetry sectors depends sensitively on  $\varphi$ .

For  $\varphi = 0$ , the initial state lies entirely in the fully symmetric Dicke manifold,  $w_{S_\varphi^2}^{\varphi=0} = 1$ , and the critical driving strength reaches its maximal value, reproducing the BTC threshold [15, 41]. As  $\varphi$  is tuned away from zero, weight is transferred into non symmetric sectors, as shown in [Fig. 2(b)]. Since different symmetry sectors are dynamically decoupled, only the component within the fully symmetric manifold undergoes the collective instability responsible for time-crystalline dynamics. The effective evolution is therefore governed by a Dicke state with reduced effective spin length, leading to a corresponding reduction of the critical driving strength [46, 64]. In the limit of  $\varphi \rightarrow \pm\pi$ , the contribution of the fully symmetric Dicke manifold vanishes  $w_{S_\varphi^2}^\varphi \rightarrow 0$ . In this regime, arbitrarily weak driving induces time-crystalline dynamics [45, 46], consistent with the vanishing threshold observed in [Fig. 2(a)]. At the exact antisymmetric point (exactly  $\varphi = \pm\pi$ ), the initial state becomes a dark state, remaining unaffected by the dissipative dynamics. Within the time-crystalline phase, both species exhibit frequency-locked oscillations that converge to the mean-field behavior as  $N$  increases [Fig. 2(c,d)]. The oscillation frequency  $\tilde{\omega}$  increases with the weight  $\bar{w}^\varphi$ , reflecting the contribution of dressed modes originating outside the fully symmetric manifold [45].

Finally, we note that the physics of the system for finite detuning  $\Delta \neq 0$  differs qualitatively. For  $\eta < \eta_c$ , the system does not relax to a stationary state but instead exhibits persistent oscillations at frequency  $\Delta$ , associated with decoherence-free subspaces corresponding to purely imaginary eigenvalues  $\pm i\Delta$ . For  $\eta > \eta_c$ , the oscillation frequencies are modified in a manner analogous to the resonant case; see [56] for details.

*Single-species three-level system and its symmetries.*— To illustrate the generality of phase-controlled strong symmetries, we consider  $N$  atoms with a common ground state  $|0\rangle$  and two excited states  $|A\rangle$  and  $|B\rangle$  [Fig. 1(c)]. Each atom is coupled to the cavity via Raman transitions with amplitudes  $g_A$  and  $g_B$ . A relative phase  $\varphi$  is imprinted by phase-shifting the Raman lasers such that  $g_A = g$  and  $g_B = ge^{-i\varphi}$ . After adiabatic elimination of the cavity, [Fig. 1(d)], the atomic dynamics is governed by

$$\dot{\hat{\mu}}_{3s} = -\frac{i}{\hbar}[\hat{H}_{3s}, \hat{\mu}_{3s}] + \frac{\Gamma}{N}\mathcal{D}[\hat{\Lambda}_\varphi]\hat{\mu}_{3s}, \quad (4)$$

where  $\hat{\mu}_{3s}$  is the reduced atomic density matrix,  $\Gamma = 4g^2/\kappa$ ,  $\hat{\Lambda}_\varphi = \hat{\Lambda}_A + e^{-i\varphi}\hat{\Lambda}_B$ , and  $\hat{\Lambda}_k = \sum_{j=1}^N |0\rangle\langle k|_j$  with  $k \in \{A, B\}$ . The effective Hamiltonian reads  $\hat{H}_{3s} = \hbar\sum_k \Delta_k \hat{\Lambda}_k^\dagger \hat{\Lambda}_k + \hbar\mathcal{E}(\hat{\Lambda}_\varphi + \hat{\Lambda}_\varphi^\dagger)$ , where  $\mathcal{E} = 2\eta g/\kappa$ .

For equal detunings,  $\Delta_A = \Delta_B = \Delta$ , the dynamics admits a phase-dependent strong symme-

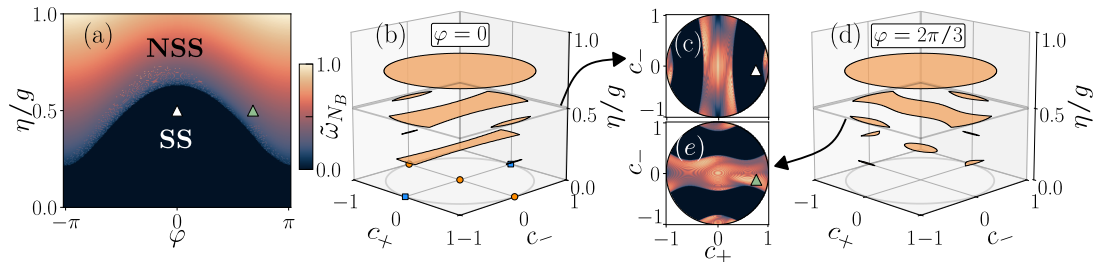


FIG. 3. **Three-level system frequency response.** (a) Phase-dependent steady-state phase diagram showcasing frequency response for a chosen initial state with  $c_{\pm} = (1 \pm \sqrt{2})/2\sqrt{2}$ ,  $c_0 = \sqrt{1 - c_+^2 - c_-^2}$ , far from the eigenstates  $|v_{\pm 1}\rangle$ . The order parameter  $\tilde{\omega}_{NB}$  is the normalized dominant Fourier component of the excited state  $B$ . (b) Initial state visualization of threshold contours in  $(c_+, c_-)$  parameter space for  $\varphi = 0$ . States are defined as nonstationary if  $\tilde{\omega}_{NB} \geq 0.01$  and shaded orange. On the  $\eta/g = 0$  plane we highlight the eigenstates of  $\hat{\tau}_j^{\varphi}$  mentioned in the main text. (c) Parameter space map taken at the  $\eta/g = 0.5$  slice from (b). (d) Threshold contours for  $\varphi = 2\pi/3$ , and the equivalent parameter space map (e). The white and green markers correspond to the initial state used in (a), falling inside the nonstationary regime as  $\varphi$  is tuned. Other parameters used  $g/\kappa = 0.1$ ,  $\Delta = 0$ , for a simulation time of  $gt = 2 \times 10^4$ .

try that can be written as a sum of single-atom operators,  $\hat{T}^{\varphi} = \sum_{j=1}^N \hat{\tau}_j^{\varphi}$ , with  $\hat{\tau}_j^{\varphi} = |0\rangle\langle 0|_j + e^{-i\varphi} |A\rangle\langle B|_j + e^{i\varphi} |B\rangle\langle A|_j$ . To elucidate the structure of the dynamically invariant subspaces, we examine the eigenstates of the single-atom operators  $\hat{\tau}_j^{\varphi}$ , which split according to their eigenvalues  $\pm 1$ :

$$|v_{+1}\rangle_j \equiv \{|0\rangle_j, |+\rangle_j\}, \quad |v_{-1}\rangle_j \equiv |-\rangle_j, \quad (5)$$

where  $|\pm\rangle_j = (|B\rangle_j \pm e^{-i\varphi} |A\rangle_j) / \sqrt{2}$ . For  $\Delta = 0$ , the states in  $|v_{+1}\rangle_j$  form a doubly-degenerate subspace in which excitations can cycle between  $|0\rangle_j$  and  $|+\rangle_j$  under the combined action of Hamiltonian and dissipative dynamics. We therefore identify this as the *bright subspace*. In contrast,  $|v_{-1}\rangle_j$  is a *dark state*, decoupled from both coherent and dissipative dynamics. Extending this structure to  $N$  atoms suggests that the population of dark states strongly influences the long time dynamics. In particular, the fraction of atoms occupying the dark subspace, together with the driving rate  $\eta$ , determine whether the system evolves toward a stationary or non-stationary phase. We quantify this dependence in the following section.

*State-space dependent dynamics.*— To illustrate the dynamical role of the bright and dark subspaces, we consider a family of pure initial states  $\hat{\mu}_{3s}(0) = |\psi_{3s}\rangle\langle\psi_{3s}|$  with  $|\psi_{3s}\rangle = c_+ |+\rangle^{\otimes N} + c_- |-\rangle^{\otimes N} + c_0 |0\rangle^{\otimes N}$ , where  $c_0 = \sqrt{1 - c_+^2 - c_-^2}$  and  $c_{\pm} \in [0, 1]$ . We quantify the support of a state on the symmetry sectors via the weights  $w_{\pm}^{\varphi} = \text{Tr}[\hat{\Pi}_{\pm}^{\varphi} \hat{\mu}_{3s}]$ , where the projectors onto the bright and dark subspaces are  $\hat{\Pi}_{\pm}^{\varphi} = \bigotimes_j^N |v_{\pm 1}\rangle\langle v_{\pm 1}|_j$ .

Non-stationary dynamics can arise either from sufficiently strong driving or from finite overlap with the freely evolving bright subspace ( $w_+^{\varphi} > 0$ ). The competition between drive and sector weight

determines the long-time behaviour, such that the critical driving strength  $\eta_c$  depends on the parameters of the initial state  $c_{\pm}$  as well as on the phase  $\varphi$ . To characterize the non-stationary phase, we analyze the mean-field dynamics with initial conditions determined by expectation values in  $|\psi_{3s}\rangle$ . As an order parameter we use the normalized dominant frequency  $\tilde{\omega}_{NB}$  of the Fourier transform of the population of the excited-state  $B$ . The choice of observable is not essential, and other choices yield equivalent results [65].

For initial states with  $0 < w_{\pm}^{\varphi} < 1$ , the behaviour closely parallels the spin-1/2 case: the critical drive  $\eta_c$  decreases monotonically as  $\varphi \rightarrow \pm\pi$  [see Fig. 3(a)]. The full mean-field phase diagram at  $\varphi = 0$  in  $(c_+, c_-, \eta)$  space is shown in [Fig. 3(b)]. Purely bright states appear at  $(c_+, c_-, 0) = (\pm 1, 0, 0)$  and  $(0, 0, 0)$ , while the many-body dark state  $|-\rangle^{\otimes N}$  lie at  $(0, \pm 1, 0)$ . As  $\eta$  increases, oscillatory regions expand from the bright subspace, forming contours with  $\tilde{\omega}_{NB} \neq 0$  [Figs. 3(b-c)]. Introducing  $\varphi \neq 0$  rotates the bright and dark subspaces in parameter space without changing their measure [Figs. 3(d-e)], redistributing the initial state weight between symmetry sectors at fixed  $\eta$ . This rotation induces transitions between stationary and time-crystalline phases and explains the phase-dependent reduction of the threshold in this three-level model. For sufficiently strong drive ( $\eta \gtrsim g/\sqrt{2}$ ), oscillations occur for all initial states. Although we focus on pure initial states, an extension to mixed states follows by convexity.

For finite detuning  $\Delta \neq 0$ , the system exhibits a decoherence-free subspace (DFS), analogous to the two-species case. For opposing detunings  $\Delta_A = -\Delta_B \equiv \Delta$ , no DFS exists at finite  $N$ . However, in the thermodynamic limit  $N \rightarrow \infty$ , eigenvalues  $\pm i\Delta$  acquire vanishing real parts. We refer to this as an

emergent DFS (eDFS), whose oscillation frequency is set solely by  $\Delta$ . Additional details are provided in the Supplemental Material [56].

*Discussion and Outlook*–. In summary, we have shown that a tunable phase provides a practical and efficient control parameter for dissipative phase transitions and long-time dynamics in open quantum systems. Its effect can be understood in terms of a phase-dependent strong symmetry that effectively rotates the invariant symmetry sectors of the Liouvillian, in turn controlling the overlap with symmetry subspaces and substantially reducing the driving threshold for non-stationary dynamics.

We demonstrated the generality of this mechanism in two cavity QED realizations of the Tavis–Cummings model, namely a two-spin-species system and a single-species three-level atomic gas. Beyond enabling controlled access to emergent dynamical phases without tailored initial-state preparation, phase control allows selective switching between protected dark and driven bright states using a single experimental parameter. This provides a versatile route to symmetry-protected storage and tunable oscillatory phases, with potential applications in quantum memories, precision timekeeping, and sensing.

*Acknowledgements*–. The research leading to these results has received funding from the Deutsche Forschungsgemeinschaft (DFG, German Research Foundation) under the Research Unit FOR 5413/1, Grant No. 465199066. P.S. acknowledges support from the Alexander von Humboldt Foundation through a Humboldt research fellowship for postdoctoral researchers.

*Data availability*–. The data that support the findings of this article are openly available [66], with an associated Github repository [67].

- 
- [1] Y. Kosmann-Schwarzbach, *The Noether Theorems: Invariance and Conservation Laws in the Twentieth Century* (Springer, 2011).
  - [2] F. Strocchi, *Symmetry breaking*, Vol. 643 (Springer, 2005).
  - [3] H.-P. Breuer and F. Petruccione, *The theory of open quantum systems* (OUP Oxford, 2002).
  - [4] R. Alicki and K. Lendi, *Quantum dynamical semigroups and applications*, Vol. 717 (Springer, 2007).
  - [5] B. Buča and T. Prosen, A note on symmetry reductions of the lindblad equation: transport in constrained open spin chains, *New J. Phys.* **14**, 073007 (2012).
  - [6] V. V. Albert and L. Jiang, Symmetries and conserved quantities in lindblad master equations, *Phys. Rev. A* **89**, 022118 (2014).
  - [7] B. Baumgartner and H. Narnhofer, Analysis of quantum semigroups with gks–lindblad generators: Ii. general, *J. Phys. A: Math. Theor.* **41**, 395303 (2008).
  - [8] L.-A. Wu and D. Lidar, Creating decoherence-free subspaces using strong and fast pulses, *Phys. Rev. Lett.* **88**, 207902 (2002).
  - [9] A. Beige, D. Braun, B. Tregenna, and P. L. Knight, Quantum computing using dissipation to remain in a decoherence-free subspace, *Phys. Rev. Lett.* **85**, 1762 (2000).
  - [10] V. V. Albert, B. Bradlyn, M. Fraas, and L. Jiang, Geometry and response of lindbladians, *Phys. Rev. X* **6**, 041031 (2016).
  - [11] D. A. Lidar and K. Birgitta Whaley, Decoherence-free subspaces and subsystems, in *Irreversible quantum dynamics* (Springer, 2003) pp. 83–120.
  - [12] A. Shabani and D. A. Lidar, Theory of initialization-free decoherence-free subspaces and subsystems, *Phys. Rev. A* **72**, 042303 (2005).
  - [13] D. M. Bacon, *Decoherence, control, and symmetry in quantum computers* (University of California, Berkeley, 2001).
  - [14] L. H. Vaecairn, J. T. Reilly, J. D. Wilson, S. B. Jäger, and M. Holland, Engineering tunable decoherence-free subspaces with collective atom-cavity interactions, *Phys. Rev. A* **111**, 033718 (2025).
  - [15] F. Iemini, A. Russomanno, J. Keeling, M. Schirò, M. Dalmonte, and R. Fazio, Boundary time crystals, *Phys. Rev. Lett.* **121**, 035301 (2018).
  - [16] H. Alaeian and B. Buča, Exact multistability and dissipative time crystals in interacting fermionic lattices, *Comms. Phys.* **5**, 318 (2022).
  - [17] B. Buča, J. Tindall, and D. Jaksch, Non-stationary coherent quantum many-body dynamics through dissipation, *Nat. Comms.* **10**, 1730 (2019).
  - [18] P. Kongkhambut, J. Skulte, L. Mathey, J. G. Cosme, A. Hemmerich, and H. Keßler, Observation of a continuous time crystal, *Science* **377**, 670 (2022).
  - [19] A. Cabot, F. Carollo, and I. Lesanovsky, Continuous sensing and parameter estimation with the boundary time crystal, *Phys. Rev. Lett.* **132**, 050801 (2024).
  - [20] D. Gribben, A. Sanpera, R. Fazio, J. Marino, and F. Iemini, Boundary time crystals as ac sensors: Enhancements and constraints, *SciPost Phys.* **18**, 100 (2025).
  - [21] F. Carollo, K. Brandner, and I. Lesanovsky, Nonequilibrium many-body quantum engine driven by time-translation symmetry breaking, *Phys. Rev. Lett.* **125**, 240602 (2020).
  - [22] M. P. Zaletel, M. Lukin, C. Monroe, C. Nayak, F. Wilczek, and N. Y. Yao, Colloquium: Quantum and classical discrete time crystals, *Rev. Mod. Phys.* **95**, 031001 (2023).
  - [23] P. J. Paulino, A. Cabot, G. De Chiara, M. Antezza, I. Lesanovsky, and F. Carollo, Thermodynamics of coupled time crystals with an application to energy storage, *Quantum Sci. Technol.* **11**, 015003 (2025).
  - [24] M.-O. Pleinert, J. von Zanthier, and G. S. Agarwal, Hyperradiance from collective behavior of coherently driven atoms, *Optica* **4**, 779 (2017).
  - [25] A. Metelmann and A. A. Clerk, Nonreciprocal photon transmission and amplification via reservoir engineering, *Phys. Rev. X* **5**, 021025 (2015).
  - [26] J. T. Young, E. Chaparro, A. Piñeiro Orioli, J. K. Thompson, and A. M. Rey, Engineering one axis

- twisting via a dissipative berry phase using strong symmetries, *Phys. Rev. Lett.* **134**, 040801 (2025).
- [27] M. Fruchart, R. Hanai, P. B. Littlewood, and V. Vitelli, Non-reciprocal phase transitions, *Nature* **592**, 363 (2021).
- [28] A. Clerk, Introduction to quantum non-reciprocal interactions: from non-hermitian hamiltonians to quantum master equations and quantum feedforward schemes, *SciPost Phys. Lect. Notes*, 044 (2022).
- [29] S. Barzanjeh, A. Xuereb, A. Alù, S. A. Mann, N. Nefedkin, V. Peano, and P. Rabl, *Nonreciprocity in quantum technology* (2025), arXiv:2508.03945 [quant-ph].
- [30] C. C. Wanjura, J. J. Slim, J. del Pino, M. Brunelli, E. Verhagen, and A. Nunnenkamp, Quadrature nonreciprocity in bosonic networks without breaking time-reversal symmetry, *Nat. Phys.* **19**, 1429 (2023).
- [31] Y.-W. Jing, H.-Q. Shi, and X.-W. Xu, Nonreciprocal photon blockade and directional amplification in a spinning resonator coupled to a two-level atom, *Phys. Rev. A* **104**, 033707 (2021).
- [32] C. Vega, A. M. de las Heras, D. Porras, and A. González-Tudela, Topological, multi-mode amplification induced by non-reciprocal, long-range dissipative couplings, *Quantum* **9**, 1861 (2025).
- [33] E. I. R. Chiacchio, A. Nunnenkamp, and M. Brunelli, Nonreciprocal dicke model, *Phys. Rev. Lett.* **131**, 113602 (2023).
- [34] T. Nadolny, C. Bruder, and M. Brunelli, Nonreciprocal synchronization of active quantum spins, *Phys. Rev. X* **15**, 011010 (2025).
- [35] G. Lyu and M.-J. Hwang, *Nonreciprocal and geometric frustration in dissipative quantum spins*, arXiv:2508.06444 [quant-ph].
- [36] J. Ho, Y.-H. Lu, T. Xiang, T.-C. Lee, Z. Yan, and D. M. Stamper-Kurn, *Higher symmetry breaking and non-reciprocity in a driven-dissipative dicke model* (2025), arXiv:2510.04288 [quant-ph].
- [37] B. Buča, J. Tindall, and D. Jaksch, Non-stationary coherent quantum many-body dynamics through dissipation, *Nat. Comms.* **10**, 1730 (2019).
- [38] B. Buča and D. Jaksch, Dissipation induced non-stationarity in a quantum gas, *Phys. Rev. Lett.* **123**, 260401 (2019).
- [39] A. Pizzi, J. Knolle, and A. Nunnenkamp, Periodic discrete time crystals and quasicrystals with ultracold bosons, *Phys. Rev. Lett.* **123**, 150601 (2019).
- [40] R. Hurtado-Gutiérrez, F. Carollo, C. Pérez-Espigares, and P. I. Hurtado, Building continuous time crystals from rare events, *Phys. Rev. Lett.* **125**, 160601 (2020).
- [41] F. Carollo and I. Lesanovsky, Exact solution of a boundary time-crystal phase transition: Time-translation symmetry breaking and non-markovian dynamics of correlations, *Phys. Rev. A* **105**, L040202 (2022).
- [42] M. Hajdušek, P. Solanki, R. Fazio, and S. Vinjanampathy, Seeding crystallization in time, *Phys. Rev. Lett.* **128**, 080603 (2022).
- [43] M. Krishna, P. Solanki, M. Hajdušek, and S. Vinjanampathy, Measurement-induced continuous time crystals, *Phys. Rev. Lett.* **130**, 150401 (2023).
- [44] Y. Nakanishi and T. Sasamoto, Dissipative time crystals originating from parity-time symmetry, *Phys. Rev. A* **107**, L010201 (2023).
- [45] F. Iemini, D. Chang, and J. Marino, Dynamics of inhomogeneous spin ensembles with all-to-all interactions: Breaking permutational invariance, *Phys. Rev. A* **109**, 032204 (2024).
- [46] P. Solanki, M. Krishna, M. Hajdušek, C. Bruder, and S. Vinjanampathy, Exotic synchronization in continuous time crystals outside the symmetric subspace, *Phys. Rev. Lett.* **133**, 260403 (2024).
- [47] A. Cabot, G. L. Giorgi, and R. Zambrini, Nonequilibrium transition between dissipative time crystals, *PRX Quantum* **5**, 030325 (2024).
- [48] R. Mattes, I. Lesanovsky, and F. Carollo, Entangled time-crystal phase in an open quantum light-matter system, *Phys. Rev. A* **108**, 062216 (2023).
- [49] A. Mukherjee, Y. Ibrahim, M. Hajdušek, and S. Vinjanampathy, Symmetries and correlations in continuous time crystals, *Phys. Rev. A* **110**, 012220 (2024).
- [50] F. Carollo, I. Lesanovsky, M. Antezza, and G. D. Chiara, Quantum thermodynamics of boundary time-crystals, *Quantum Sci. Technol.* **9**, 035024 (2024).
- [51] P. J. Paulino, I. Lesanovsky, and F. Carollo, Nonequilibrium thermodynamics and power generation in open quantum optomechanical systems, *Phys. Rev. A* **108**, 023516 (2023).
- [52] F. Russo and T. Pohl, Quantum dissipative continuous time crystals, *Phys. Rev. Lett.* **135**, 110404 (2025).
- [53] Z. Wang, R. Gao, X. Wu, B. Buča, K. Mølmer, L. You, and F. Yang, Boundary time crystals induced by local dissipation and long-range interactions, *Phys. Rev. Lett.* **135**, 230401 (2025).
- [54] P. Solanki, A. Cabot, M. Brunelli, F. Carollo, C. Bruder, and I. Lesanovsky, Generation of entanglement and nonstationary states via competing coherent and incoherent bosonic hopping, *Phys. Rev. A* **112**, L030601 (2025).
- [55] J. C. Schumann, I. Lesanovsky, and P. Solanki, *Hierarchical time crystals* (2026), arXiv:2601.09779 [quant-ph].
- [56] See Supplemental Material for further details about the microscopic derivation, the atom-only models and spectral properties in wider parameter regimes. The Supplemental includes Refs. [3, 57–63].
- [57] M. Nairn, L. Giannelli, G. Morigi, S. Slama, B. Olmos, and S. B. Jäger, Spin self-organization in an optical cavity facilitated by inhomogeneous broadening, *Phys. Rev. Lett.* **134**, 083603 (2025).
- [58] F. Mivehvar, F. Piazza, T. Donner, and H. Ritsch, Cavity QED with quantum gases: New paradigms in many-body physics, *Adv. Phys.* **70**, 1 (2021).
- [59] R. Azouit, A. Sarlette, and P. Rouchon, Adiabatic elimination for open quantum systems with effective lindblad master equations, in *2016 IEEE 55th Conference on Decision and Control (CDC)* (IEEE, 2016) pp. 4559–4565.
- [60] D. J. Griffiths and D. F. Schroeter, *Introduction to quantum mechanics* (Cambridge university press, 2018).
- [61] F. Minganti, A. Biella, N. Bartolo, and C. Ciuti, Spectral theory of liouvillians for dissipative phase transitions, *Phys. Rev. A* **98**, 042118 (2018).

- [62] H. Carmichael, Analytical and numerical results for the steady state in cooperative resonance fluorescence, *J. Phys. B: Atom. Mol. Phys.* **13**, 3551 (1980).
- [63] R. H. Dicke, Coherence in spontaneous radiation processes, *Phys. Rev.* **93**, 99 (1954).
- [64] A. Cabot, F. Carollo, and I. Lesanovsky, Exploiting nonequilibrium phase transitions and strong symmetries for continuous measurement of collective observables, *Phys. Rev. A* **110**, L060601 (2024).
- [65] L. F. d. Prazeres, L. d. S. Souza, and F. Iemini, Boundary time crystals in collective d-level systems, *Phys. Rev. B* **103**, 184308 (2021).
- [66] M. Nairn, B. Olmos, and P. Solanki, Dataset for “Controlling emergent dynamical behavior via phase-engineered strong symmetries”, Zenodo (2026).
- [67] M. Nairn, [phase.strong.sym](#), GitHub (2026), accessed: 2026-02-20.

# Supplemental Material: Controlling emergent dynamical behavior via phase-engineered strong symmetries

Marc Nairn, Beatriz Olmos, and Parvinder Solanki

*Institut für Theoretische Physik, Universität Tübingen, Auf der Morgenstelle 14, 72076 Tübingen, Germany*

## I. MICROSCOPIC DERIVATION OF THE MODELS

In this section, we outline all the necessary steps to derive the Hamiltonians introduced in the main text. For this, we start with multilevel atoms that have either two independent ground states or a common ground state, yielding either the two-species spin-1/2 system or the collective three-level system, respectively.

*Two-species spin-1/2 systems*–. First, we consider the two-species spin-1/2 systems. The single-particle Hamiltonian for each spin species coupled to a shared cavity mode with annihilation operator  $\hat{a}$  can be written as

$$H = H_0 + H_{at} + H_{ac} + H_d. \quad (\text{S1})$$

The free Hamiltonian is

$$H_0 = \omega_c \hat{a}^\dagger \hat{a} + \sum_{m=A,B} (\omega_r |r\rangle\langle r|_m + \omega_s |s\rangle\langle s|_m + \omega_m |\uparrow\rangle\langle\uparrow|_m), \quad (\text{S2})$$

where  $\omega_c$  is the cavity frequency,  $\omega_r, \omega_s$  are the excited-state energies (for the two Raman intermediate states), and  $\omega_m$  denotes the bare energy of the  $|\uparrow\rangle_m$  level for species  $m$ .

The Raman laser couplings are

$$H_{at} = \left( \frac{\Omega_r}{2} e^{-i\omega_{lr}t} |r\rangle\langle\downarrow|_A + \frac{\Omega_s}{2} e^{-i\omega_{ls}t} |s\rangle\langle\downarrow|_B + \text{h.c.} \right), \quad (\text{S3})$$

and the atom–cavity dipole couplings are

$$H_{ac} = (\lambda_r |\uparrow\rangle\langle r|_A \hat{a} + \lambda_s |\uparrow\rangle\langle s|_B \hat{a} + \text{h.c.}). \quad (\text{S4})$$

Finally, the cavity is driven by

$$H_d = i\eta (e^{i\omega_{ld}t} \hat{a}^\dagger - e^{-i\omega_{ld}t} \hat{a}), \quad (\text{S5})$$

with drive amplitude  $\eta$  and drive frequency  $\omega_{ld}$ . The laser Rabi frequencies  $\Omega_r, \Omega_s$  are in general complex-valued (we will keep magnitudes and phases implicit).

We remove explicit time dependence using a diagonal operator  $K$  by introducing the unitary

$$U(t) = e^{iKt}, \quad H' \equiv U H U^\dagger - K, \quad (\text{S6})$$

where

$$K = \omega_{ld} \hat{a}^\dagger \hat{a} + \omega_{lr} |r\rangle\langle r|_A + \omega_{ls} |s\rangle\langle s|_B + (\omega_{lr} - \omega_{ld}) |\uparrow\rangle\langle\uparrow|_A + (\omega_{ls} - \omega_{ld}) |\uparrow\rangle\langle\uparrow|_B. \quad (\text{S7})$$

The time-independent Hamiltonian becomes

$$H' = \Delta_c \hat{a}^\dagger \hat{a} + \delta_r |r\rangle\langle r|_A + \delta_s |s\rangle\langle s|_B + \delta_A |\uparrow\rangle\langle\uparrow|_A + \delta_B |\uparrow\rangle\langle\uparrow|_B + \left( \frac{\Omega_r}{2} |r\rangle\langle\downarrow|_A + \frac{\Omega_s}{2} |s\rangle\langle\downarrow|_B + \lambda_r |\uparrow\rangle\langle r|_A \hat{a} + \lambda_s |\uparrow\rangle\langle s|_B \hat{a} + \text{h.c.} \right) + i\eta (\hat{a}^\dagger - \hat{a}), \quad (\text{S8})$$

where we have introduced the detunings

$$\begin{aligned} \Delta_c &= \omega_c - \omega_{ld}, & \delta_r &= (\omega_r - \omega_{lr}), & \delta_s &= (\omega_s - \omega_{ls}), \\ \delta_A &= (\omega_A - \omega_{lr}) + \omega_{ld}, & \delta_B &= (\omega_B - \omega_{ls}) + \omega_{ld}. \end{aligned} \quad (\text{S9})$$

We now eliminate  $|r\rangle$  and  $|s\rangle$  perturbatively under the standard large single-photon detuning assumptions:

$$|\delta_r| \gg |\Omega_r|, |\lambda_r| \quad |\delta_s| \gg |\Omega_s|, |\lambda_s|. \quad (\text{S10})$$

We can thus write  $H' = |\mathcal{S}\rangle\langle\mathcal{S}| + |\mathcal{F}\rangle\langle\mathcal{F}| + |\mathcal{S}\rangle\langle\mathcal{F}| + |\mathcal{F}\rangle\langle\mathcal{S}|$  for the slow ( $\mathcal{S}$ ) and fast ( $\mathcal{F}$ ) evolving subspaces spanned by the cavity + low lying electronic states ( $|\uparrow\rangle_m, |\downarrow\rangle_m$ ), and the far detuned states ( $|r\rangle, |s\rangle$ ), respectively. The effective Hamiltonian up to first order in  $(\delta_{r,s})^{-1}$  for the slow subspace is given by

$$H_{\text{eff}} = |\mathcal{S}\rangle\langle\mathcal{S}| - |\mathcal{S}\rangle\langle\mathcal{F}| (|\mathcal{F}\rangle\langle\mathcal{F}|)^{-1} |\mathcal{F}\rangle\langle\mathcal{S}|$$

which accounts for the coherent two-photon coupling between  $|\downarrow\rangle$  and  $|\uparrow\rangle$  mediated by  $|r\rangle, |s\rangle$ , and the AC Stark and dispersive shifts of the atomic levels. The resulting effective Hamiltonian (dropping constant energy terms) reads

$$H_{\text{eff}} = \Delta_c \hat{a}^\dagger \hat{a} + \sum_{m=A,B} (U_m \hat{a}^\dagger \hat{a} |\uparrow\rangle\langle\uparrow|_m + V_m |\downarrow\rangle\langle\downarrow|_m) + (g_m \hat{a} |\uparrow\rangle\langle\downarrow|_m + \text{h.c.}) + i\eta (\hat{a}^\dagger - \hat{a}). \quad (\text{S11})$$

Here the single atom-cavity couplings are  $g_A \simeq -\frac{\lambda_r \Omega_r^*}{2\delta_r}$ ,  $g_B \simeq -\frac{\lambda_s \Omega_s^*}{2\delta_s}$ , and the leading AC Stark and dispersive shifts are given by

$$V_A \simeq \omega_A - \frac{|\Omega_r|^2}{4\delta_r}, \quad U_A \simeq -\frac{|\lambda_r|^2}{\delta_r}, \\ V_B \simeq \omega_B - \frac{|\Omega_s|^2}{4\delta_s}, \quad U_B \simeq -\frac{|\lambda_s|^2}{\delta_s}.$$

To obtain the Hamiltonian used in the main text, we have discarded the  $U_m$  contributions assuming to be working in the bad-cavity regime, where dispersive effects are negligible [57, 58]. We set a relative phase in the Raman lasers

$$\Omega_r = |\Omega_r|, \quad \Omega_s = |\Omega_r| e^{i\varphi} \quad (\text{S12})$$

such that  $g_A = |g_A| \equiv g$ ,  $g_B = g e^{-i\varphi}$ . Extending this approach to an atomic ensemble, we arrive at the form shown in the main text

$$H_2 = \hbar \Delta_c \hat{a}^\dagger \hat{a} + i\hbar \sqrt{N} \eta (\hat{a}^\dagger - \hat{a}) + \hbar \left( \sum_m \Delta_m \hat{S}_m^z \right) + \frac{\hbar g}{\sqrt{N}} (\hat{a}^\dagger \hat{S}_\varphi + \hat{a} \hat{S}_\varphi^\dagger), \quad (\text{S13})$$

with  $\Delta_m \approx -V_m$ . Here we have used the collective spin operators

$$\hat{S}_m^z = \frac{1}{2} \sum_{j=1}^{N/2} (\hat{\sigma}_{j,m}^\dagger \hat{\sigma}_{j,m} - \hat{\sigma}_{j,m} \hat{\sigma}_{j,m}^\dagger), \quad \text{and} \quad \hat{S}_\varphi = \sum_{j=1}^{N/2} \hat{\sigma}_{jA} + e^{-i\varphi} \sum_{j=1}^{N/2} \hat{\sigma}_{jB}$$

with  $\hat{\sigma}_{jm} = |\uparrow\rangle\langle\downarrow|_{jm}$ .

*Multilevel system with common ground state*-. We now focus on deriving the effective Hamiltonian for the collective three-level case. We consider a 5-level system as shown in Fig. S1(b), which can be seen as a combination of both spin-1/2 species sharing a common ground state given by  $|0\rangle$ , mapping to an effective spin-1 system. In analogy with the two spin-1/2 systems, the Hamiltonian for now reads as

$$H = H_0 + H_{at} + H_{ac} + H_d \quad (\text{S14})$$

with the free Hamiltonian

$$H_0 = \omega_c \hat{a}^\dagger \hat{a} + (\{\omega_r |r\rangle\langle r| + \omega_s |s\rangle\langle s| + \omega_B |B\rangle\langle B| + \omega_A |A\rangle\langle A|}), \quad (\text{S15})$$

internal laser driving,

$$H_{at} = \frac{\Omega_r}{2} e^{-i\omega_r t} |r\rangle\langle 0| + \frac{\Omega_s}{2} e^{-i\omega_s t} |s\rangle\langle 0| + \text{h.c.} \quad \text{where } \Omega_r, \Omega_s \in \mathbb{C}^+, \quad (\text{S16})$$

atom-cavity transitions

$$H_{ac} = [(\lambda_r |A\rangle\langle r| \hat{a} + \lambda_s |B\rangle\langle s| \hat{a}) + \text{h.c.}], \quad (\text{S17})$$

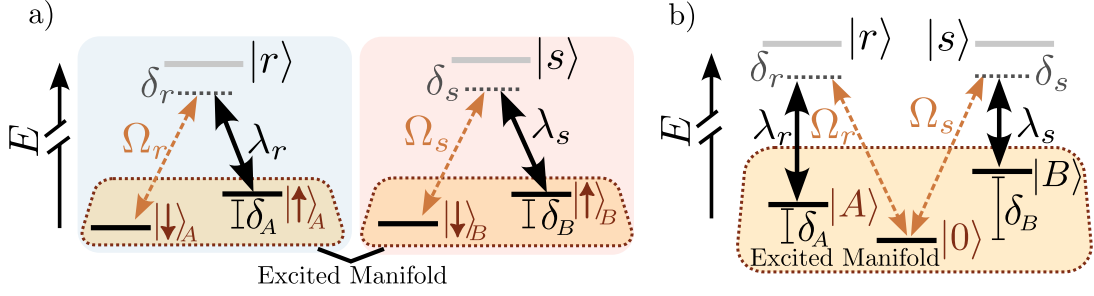


FIG. S1. **Raman level schemes.** (a) Two multilevel atomic species ( $A, B$ ) with distinct ground states and (b) with a shared ground state. Frequencies  $\Omega_{r,s}$  drive the optical transitions between the ground and a far detuned ( $\delta_{r,s} \gg \Omega_{r,s}$ ) state  $|r, s\rangle$ . The cavity couples with strength  $\lambda_{r,s}$  to a low lying excited state detuned from the ground state by  $\delta_{A/B}$  via a consequent emission/absorption of a photon  $\hat{a}$  ( $\hat{a}^\dagger$ ). The dynamics of interest is contained in the low-lying energetic states. We can embed a relative phase in the system by setting  $\Omega_{r,s} = |\Omega_{r,s}|e^{i\varphi_{r,s}}$ : without loss of generality we choose  $|\Omega_r| = |\Omega_s|$ , for  $\varphi_r = 0$  and  $\varphi_s \equiv \varphi$ .

and the external cavity driving term

$$H_d = i\eta (e^{i\omega_d t} \hat{a}^\dagger - e^{-i\omega_d t} \hat{a}). \quad (\text{S18})$$

Similar to the previous case, we can write the interaction picture Hamiltonian with respect to the driving lasers,

$$\tilde{H} = \Delta_c \hat{a}^\dagger \hat{a} + i\eta (\hat{a}^\dagger - \hat{a}) + \left\{ \sum_{\mu=r,s,A,B} \delta_\mu |\mu\rangle\langle\mu| + \frac{\Omega_r}{2} |r\rangle\langle 0| + \frac{\Omega_s}{2} |s\rangle\langle 0| + (\lambda_r |A\rangle\langle r| \hat{a} + \lambda_s |B\rangle\langle s| \hat{a}) + \text{h.c.} \right\} \quad (\text{S19})$$

with detunings

$$\begin{aligned} \Delta_c &= \omega_c - \omega_{ld}, & \delta_r &= \omega_r - \omega_{lr}, & \delta_s &= \omega_s - \omega_{ls}, \\ \delta_A &= (\omega_A - \omega_{lr}) + \omega_{ld}, & \delta_B &= (\omega_B - \omega_{ls}) + \omega_{ld}. \end{aligned} \quad (\text{S20})$$

Following similar steps as before, we can eventually arrive at the description for the low-lying state manifold dynamics given by the effective Hamiltonian

$$H_{\text{eff}} = \Delta_c \hat{a}^\dagger \hat{a} + i\eta (\hat{a}^\dagger - \hat{a}) + \sum_{m=A,B} (\Delta_m + U_m \hat{a}^\dagger \hat{a}) |m\rangle\langle m| + g_m \hat{a} |m\rangle\langle 0| + g_m^* \hat{a}^\dagger |0\rangle\langle m| \quad (\text{S21})$$

where

$$g_A = -\frac{\Omega_r \lambda_r^*}{2\delta_r}, \quad g_B = -\frac{\Omega_s \lambda_s^*}{2\delta_s}, \quad U_A = -\frac{|\lambda_r|^2}{\delta_r}, \quad U_B = -\frac{|\lambda_s|^2}{\delta_s}, \quad \Delta_m = \delta_m + \frac{|\Omega_r|^2}{4\delta_r} + \frac{|\Omega_s|^2}{4\delta_s}.$$

Moving to a suitable chosen basis, discarding the dispersive  $U_m$  correction terms as before, and extending the model to  $N$  particles, we recover the Hamiltonian reported in the main text

$$H_{3T} = \hbar \Delta_c \hat{a}^\dagger \hat{a} + i\hbar \sqrt{N} \eta (\hat{a}^\dagger - \hat{a}) + \hbar \sum_{m=A,B} (\Delta_m \hat{N}_m) + \frac{\hbar g}{\sqrt{N}} (\hat{a} \hat{\Lambda}_\varphi^\dagger + \hat{a}^\dagger \hat{\Lambda}_\varphi), \quad (\text{S22})$$

where we have used the shorthand

$$\hat{N}_A = \sum_j \frac{\mathbb{I}_j}{3} + \hat{\lambda}_j^3 + \frac{1}{\sqrt{3}} \hat{\lambda}_j^8, \quad \hat{N}_B = \sum_j \frac{\mathbb{I}_j}{3} - \frac{2}{\sqrt{3}} \hat{\lambda}_j^8, \quad \hat{\Lambda}_A = \sum_j (\hat{\lambda}_1^j - i \hat{\lambda}_2^j), \quad \hat{\Lambda}_B = \sum_j (\hat{\lambda}_6^j - i \hat{\lambda}_7^j)$$

with relation  $\hat{\Lambda}_m^\dagger \hat{\Lambda}_m = \hat{N}_m$  to label the populations in the  $m$ -th excited leg and the operators responsible for the transition matrix elements  $|m\rangle\langle 0|$ , in terms of the Gell-Mann matrices  $\hat{\lambda}_k$  as defined in Eq. (S64). We have similarly used the collective operators introduced in the main text  $\hat{\Lambda}_\varphi = \hat{\Lambda}_A + e^{-i\varphi} \hat{\Lambda}_B$ .

## II. SEMICLASSICAL EQUATIONS OF MOTION FOR THE TWO-SPECIES MODEL

As stated in the main text, to map out the phase diagram we solve the semiclassical equations of motion obtained under a mean-field ansatz, which become exact in the thermodynamic limit  $N \rightarrow \infty$ . Using  $g_A = |g_A| = g$ ,  $g_B = e^{-i\varphi}$  they become,

$$\begin{aligned}
\dot{s}_A^x &= -\Delta_A s_A^y + i g s_A^z (\alpha - \alpha^*) \\
\dot{s}_B^x &= -\Delta_B s_B^y + i g s_B^z (e^{i\varphi} \alpha - e^{-i\varphi} \alpha^*) \\
\dot{s}_A^y &= \Delta_A s_A^x - g s_A^z (\alpha^* + \alpha) \\
\dot{s}_B^y &= \Delta_B s_B^x - g s_B^z (e^{-i\varphi} \alpha^* + e^{i\varphi} \alpha) \\
\dot{s}_A^z &= -i g s_A^x (\alpha - \alpha^*) + g s_A^y (\alpha^* + \alpha) \\
\dot{s}_B^z &= -i g s_B^x (e^{i\varphi} \alpha - e^{-i\varphi} \alpha^*) + g s_B^y (e^{-i\varphi} \alpha^* + e^{i\varphi} \alpha) \\
\dot{\alpha} &= -\left(i\Delta_c + \frac{\kappa}{2}\right) \alpha - \frac{g}{2} (i(s_A^x + e^{-i\varphi} s_B^x) + (s_A^y + e^{-i\varphi} s_B^y)) + \eta
\end{aligned} \tag{S23}$$

with  $\alpha = \langle \hat{a} \rangle / \sqrt{N}$  and  $s_m^\mu = \langle \hat{S}_m^\mu \rangle / (N/2)$  for  $m = A, B$  where  $\hat{S}^\mu = \sum_j^{N/2} \hat{\sigma}_j^{(\mu=x,y,z)}$  are the Pauli operators for the collective spins.

## III. EFFECTIVE ATOM-ONLY DESCRIPTION

In this section, we detail the steps required to obtain the effective master equation for the atomic degrees of freedom alone [59].

In the following, we consider the cavity mode  $\hat{a}$  with detuning  $\Delta_c$ , which couples to a collective atomic operator  $\hat{J}$  of  $N$  atoms via a Tavis-Cummings type interaction with coupling constant  $g/\sqrt{N}$ . The cavity is driven with strength  $\sqrt{N}\eta$  and decays at rate  $\kappa$ . For the spin-1/2 model  $\hat{J} = \hat{S}_\varphi$  whilst for the spin-1 case it is just replaced by  $\hat{J} = \hat{\Lambda}_\varphi$ .

Note we keep the free atomic evolution  $\hat{H}_{\text{at}}$  out of this description as it already lives in the reduced atom-only subspace. The full Liouvillian reads

$$\dot{\hat{\rho}} = (\mathcal{L}_0 + \mathcal{L}_1)\hat{\rho}, \tag{S24}$$

where

$$\mathcal{L}_0 \hat{\rho} = -i[\Delta_c \hat{a}^\dagger \hat{a} + i\sqrt{N}(\eta \hat{a}^\dagger - \eta^* \hat{a}), \hat{\rho}] + \kappa \mathcal{D}[\hat{a}]\hat{\rho}, \tag{S25}$$

$$\mathcal{L}_1 \hat{\rho} = \frac{-ig}{\sqrt{N}} [\hat{J} \hat{a}^\dagger + \hat{J}^\dagger \hat{a}, \hat{\rho}]. \tag{S26}$$

Here  $\mathcal{L}_0$  describes the cavity degrees of freedom (free cavity Hamiltonian, coherent drive and decay) and describes the fast dynamics, while  $\mathcal{L}_1$  contains the atom-cavity coupling and acts as a slow perturbation. Adiabatic elimination of the cavity is justified when the cavity relaxes much faster than the atomic degrees of freedom, i.e., when the perturbation is small compared to the cavity Liouvillian:

$$\|\mathcal{L}_1\| \ll \|\mathcal{L}_0\|. \tag{S27}$$

A convenient explicit condition is

$$\kappa, |\Delta_c| \gg \frac{g}{\sqrt{N}} \tag{S28}$$

In the near-resonant case ( $|\Delta_c| \lesssim \kappa$ ), this reduces to  $\kappa$  being the dominant rate. Under these conditions, the cavity reaches a quasi-steady state on a timescale ( $\tau_c \sim 1/\max(\kappa, |\Delta_c|)$ ) and can be adiabatically eliminated by projecting onto the cavity steady state and performing a perturbative expansion in  $\mathcal{L}_1$ .

To proceed with the elimination and isolate the slow atomic dynamics, we move to a displaced frame defined by

$$\hat{\rho}' = D^\dagger(\alpha) \hat{\rho} D(\alpha), \quad \text{with} \quad D(\alpha) = e^{\alpha \hat{a}^\dagger - \alpha^* \hat{a}}. \tag{S29}$$

In this frame,  $D^\dagger(\alpha)\hat{a}D(\alpha) = \hat{a} + \alpha \equiv \delta\hat{a}$ . Choosing  $\alpha = \frac{\sqrt{N}\eta}{i\Delta_c + \kappa/2}$  removes the linear drive term and simplifies the Liouvillian to

$$\mathcal{L}'_0\hat{\rho} = -i[\Delta_c \delta\hat{a}^\dagger\delta\hat{a}, \hat{\rho}] + \kappa\mathcal{D}[\delta\hat{a}]\hat{\rho}, \quad (\text{S30})$$

$$\mathcal{L}'_1\hat{\rho} = -ig_N[\hat{J}(\alpha^* + \delta\hat{a}^\dagger) + \hat{J}^\dagger(\alpha + \delta\hat{a}), \hat{\rho}]. \quad (\text{S31})$$

where we have defined  $g_N = g/\sqrt{N}$ . We separate the interaction part into a *coherent drive* and a *fluctuation* term:

$$\mathcal{L}'_1 = \mathcal{L}_1^{(\text{drive})} + \mathcal{L}_1^{(\delta)}, \quad (\text{S32})$$

$$\mathcal{L}_1^{(\text{drive})}\hat{\rho} = -i[H_{\text{drive}}, \hat{\rho}], \quad H_{\text{drive}} = g_N(\alpha^*\hat{J} + \alpha\hat{J}^\dagger), \quad (\text{S33})$$

$$\mathcal{L}_1^{(\delta)}\hat{\rho} = -ig_N[\hat{J}\delta\hat{a}^\dagger + \hat{J}^\dagger\delta\hat{a}, \hat{\rho}]. \quad (\text{S34})$$

To discern between the relevant subspaces, we define the projector  $\mathcal{P}$ , where

$$\mathcal{P}\hat{\rho} = \text{Tr}_a[\hat{\rho}] \otimes |0\rangle\langle 0|,$$

and its complement  $\mathcal{Q} = \mathbb{I} - \mathcal{P}$ . The cavity steady state in the displaced frame is the vacuum  $|0\rangle$  of  $\delta\hat{a}$ . The projector properties imply:

$$\mathcal{P}\mathcal{L}_1^{(\text{drive})}\mathcal{P} = \mathcal{L}_1^{(\text{drive})}\mathcal{P}, \quad \mathcal{P}\mathcal{L}_1^{(\delta)}\mathcal{P} = 0. \quad (\text{S35})$$

Now using the standard Nakajima–Zwanzig expansion up to second order [3], we obtain the dynamics for the reduced density matrix  $\hat{\mu} = \mathcal{P}\hat{\rho}$ :

$$\dot{\hat{\mu}} = \mathcal{P}\mathcal{L}_1^{(\text{drive})}\mathcal{P}\hat{\rho} + \int_0^\infty dt \mathcal{P}\mathcal{L}_1^{(\delta)}e^{\mathcal{L}'_0 t}\mathcal{L}_1^{(\delta)}\mathcal{P}\hat{\rho}. \quad (\text{S36})$$

We now evaluate the terms appearing in this equation. Noting that

$$\mathcal{L}_1^{(\delta)}\hat{\rho} = -ig_N[\hat{V}, \hat{\rho}], \quad \text{with } \hat{V} = \hat{J}\delta\hat{a}^\dagger + \hat{J}^\dagger\delta\hat{a}, \quad (\text{S37})$$

We can find

$$\mathcal{L}_1^{(\delta)}e^{\mathcal{L}'_0 t}\mathcal{L}_1^{(\delta)}\hat{\rho} = (-ig_N)^2[\hat{V}, e^{\mathcal{L}'_0 t}[\hat{V}, \hat{\rho}]] = -g_N^2[\hat{V}, [\hat{V}(t), \hat{\rho}]], \quad (\text{S38})$$

where  $\hat{V}(t) = e^{\mathcal{L}'_0 t}\hat{V}$ . Expanding the double commutator explicitly gives

$$[\hat{V}, [\hat{V}(t), \hat{\rho}]] = \hat{V}\hat{V}(t)\hat{\rho} - \hat{V}\hat{\rho}\hat{V}(t) - \hat{V}(t)\hat{\rho}\hat{V} + \hat{\rho}\hat{V}(t)\hat{V}. \quad (\text{S39})$$

Now further expanding  $\hat{V} = \hat{J}\delta\hat{a}^\dagger + \hat{J}^\dagger\delta\hat{a}$  and  $\hat{V}(t) = \hat{J}\delta\hat{a}^\dagger(t) + \hat{J}^\dagger\delta\hat{a}(t)$ :

$$\hat{V}\hat{V}(t)\hat{\rho} = (\hat{J}\delta\hat{a}^\dagger + \hat{J}^\dagger\delta\hat{a})(\hat{J}\delta\hat{a}^\dagger(t) + \hat{J}^\dagger\delta\hat{a}(t))\hat{\rho}, \quad (\text{S40})$$

$$\hat{V}\hat{\rho}\hat{V}(t) = (\hat{J}\delta\hat{a}^\dagger + \hat{J}^\dagger\delta\hat{a})\hat{\rho}(\hat{J}\delta\hat{a}^\dagger(t) + \hat{J}^\dagger\delta\hat{a}(t)), \quad (\text{S41})$$

$$\hat{V}(t)\hat{\rho}\hat{V} = (\hat{J}\delta\hat{a}^\dagger(t) + \hat{J}^\dagger\delta\hat{a}(t))\hat{\rho}(\hat{J}\delta\hat{a}^\dagger + \hat{J}^\dagger\delta\hat{a}), \quad (\text{S42})$$

$$\hat{\rho}\hat{V}(t)\hat{V} = \hat{\rho}(\hat{J}\delta\hat{a}^\dagger(t) + \hat{J}^\dagger\delta\hat{a}(t))(\hat{J}\delta\hat{a}^\dagger + \hat{J}^\dagger\delta\hat{a}). \quad (\text{S43})$$

Multiplying out gives sixteen terms; we only keep those that survive the trace over the cavity vacuum, i.e. those containing expectation values of the form  $\langle\delta\hat{a}(t)\delta\hat{a}^\dagger\rangle$  or  $\langle\delta\hat{a}^\dagger(t)\delta\hat{a}\rangle$ . The non-vanishing expectation values are

$$\langle 0|\delta\hat{a}(t)\delta\hat{a}^\dagger|0\rangle = e^{-(i\Delta_c + \kappa/2)t}, \quad (\text{S44})$$

$$\langle 0|\delta\hat{a}^\dagger(t)\delta\hat{a}|0\rangle = 0. \quad (\text{S45})$$

After tracing over the cavity, we obtain

$$\text{Tr}_a[\hat{V}\hat{V}(t)\hat{\rho}] \rightarrow \hat{J}\hat{J}^\dagger e^{-(i\Delta_c + \kappa/2)t}\hat{\mu}_s, \quad (\text{S46})$$

$$\text{Tr}_a[\hat{V}\hat{\rho}\hat{V}(t)] \rightarrow \hat{J}\hat{\mu}_s\hat{J}^\dagger e^{-(i\Delta_c + \kappa/2)t}, \quad (\text{S47})$$

$$\text{Tr}_a[\hat{V}(t)\hat{\rho}\hat{V}] \rightarrow \hat{J}^\dagger\hat{\mu}_s\hat{J}e^{(i\Delta_c - \kappa/2)t}, \quad (\text{S48})$$

$$\text{Tr}_a[\hat{\rho}\hat{V}(t)\hat{V}] \rightarrow \hat{\mu}_s\hat{J}^\dagger\hat{J}e^{(i\Delta_c - \kappa/2)t}. \quad (\text{S49})$$

where  $\hat{\mu}_s = \text{Tr}_a[\hat{\rho}]$  is the reduced density matrix for spin-only subsystems. Plugging all into the expression for  $\mathcal{P}\mathcal{L}_1^{(\delta)}e^{\mathcal{L}'_0 t}\mathcal{L}_1^{(\delta)}\mathcal{P}\hat{\rho}$ , we get

$$\dot{\hat{\mu}}_s = -g_N^2 \int_0^\infty dt \left( [\hat{J}, \hat{J}^\dagger(t)\hat{\mu}_s] \langle \delta\hat{a}(t)\delta\hat{a}^\dagger \rangle + [\hat{J}^\dagger, \hat{J}(t)\hat{\mu}_s] \langle \delta\hat{a}^\dagger(t)\delta\hat{a} \rangle + \text{H.c.} \right). \quad (\text{S50})$$

Since  $\langle \delta\hat{a}^\dagger(t)\delta\hat{a} \rangle = 0$  for the vacuum bath, only the first correlation contributes. Therefore

$$\dot{\hat{\mu}}_s = -g_N^2 \int_0^\infty dt e^{-(i\Delta_c + \kappa/2)t} \left( [\hat{J}, \hat{J}^\dagger\hat{\mu}_s] + [\hat{J}\hat{\mu}_s, \hat{J}^\dagger] \right). \quad (\text{S51})$$

The time integral gives

$$\int_0^\infty e^{-(i\Delta_c + \kappa/2)t} dt = \frac{1}{\kappa/2 + i\Delta_c}.$$

The above integral can be further simplify by separating real and imaginary parts as follow

$$\frac{1}{\kappa/2 + i\Delta_c} = \frac{\kappa/2 - i\Delta_c}{(\kappa/2)^2 + \Delta_c^2}.$$

Hence, the final effective Liouvillian is

$$\dot{\hat{\mu}} = -i[H_{\text{at}} + H_{\text{drive}} + H_{\text{LS}}, \hat{\mu}] + \frac{\Gamma}{N} \mathcal{D}[\hat{J}]\hat{\mu}, \quad (\text{S52})$$

where

$$H_{\text{drive}} = g\eta \left( \bar{\chi}\hat{J} + \bar{\chi}^*\hat{J}^\dagger \right), \quad \bar{\chi} = \frac{1}{\kappa/2 + i\Delta_c}, \quad (\text{S53})$$

$$H_{\text{LS}} = -\frac{g^2}{N}\Delta_c |\bar{\chi}|^2 \hat{J}^\dagger \hat{J}, \quad (\text{S54})$$

$$\Gamma = g^2\kappa |\bar{\chi}|^2. \quad (\text{S55})$$

The first term represents the coherent drive ( $H_{\text{drive}}$ ) from the cavity field amplitude, the second term given by  $H_{\text{LS}}$  is the cavity-induced Lamb shift, and the last term describes the effective decay rate  $\Gamma$  of the spin subsystems through the lossy cavity.

The validity of this effective description rests on a clear separation of timescales. In particular, the cavity must relax much faster than the atomic dynamics it induces. Once the effective model is obtained, it further demands that all induced atomic rates remain slow compared with the eliminated cavity mode, namely

$$\left\{ |g\eta\bar{\chi}|, |g^2\Delta_c|/[N(\kappa^2/4 + \Delta_c^2)], \Gamma \right\} \ll \max(\kappa, |\Delta_c|). \quad (\text{S56})$$

Under these conditions the cavity adiabatically follows its steady state, and the reduced atomic master equation above provides an accurate description of the dynamics. Substituting the suitable  $\hat{H}_{\text{at}}$  and atomic operator  $\hat{J}$  into (S52) we recover Eqs. (4) and (5) used in the main text for the spin-1/2 and spin-1 models.

#### IV. EFFECT OF FINITE CAVITY DETUNING IN TWO-SPECIES CASE

In the main text, we assumed the cavity linewidth is much larger than any relevant frequency scale so that the laser frequency and dispersive shifts,  $\Delta_c \ll \kappa$ , are neglected. In practice, this means the coherent Lamb shifts are suppressed and the dissipative terms at rate  $\Gamma$  govern the excitation exchange dynamics. For completeness we benchmark our results and can confirm the inclusion of finite cavity detuning does not alter our findings, as can be seen from Fig. S2 where the frequency peaks and frequency-matched oscillations remain even at sizeable cavity detunings. Most importantly, the sectors the strong symmetry generator partitions the dynamics into is independent of  $\Delta_c$ .

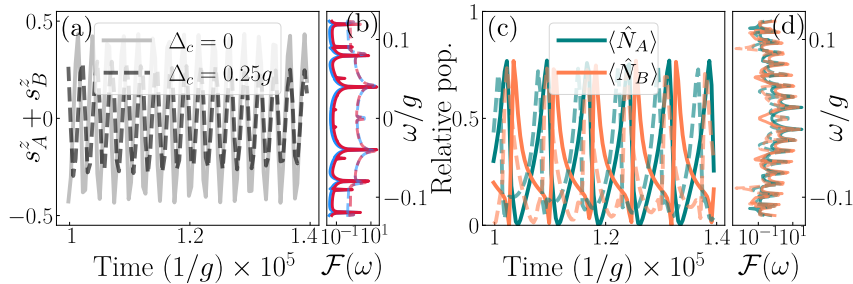


FIG. S2. **Effect of finite cavity detuning.** (a) Semiclassical dynamics of the total magnetization  $s_A^z + s_B^z$  deep into the steady state window for the  $\Delta_A = \Delta_B = 0$ ,  $\varphi = 4\pi/5$ ,  $\eta = 0.8g$  point from Fig. 2 in the main text, with and without cavity detuning, and (b) Fourier-domain comparison for each spin species (blue and red) with (dashed) and without (solid) cavity detuning. (c) Dynamics for the excited state populations of the three-level system ( $\hat{N}_k = \hat{\Lambda}_k^\dagger \hat{\Lambda}_k$ ), for an initial state parametrized with  $c_+ = 0.9/\sqrt{2}$  and  $c_- = 0.7/\sqrt{2}$  for the eigenstate populations introduced in the main text, and  $\varphi = 2\pi/3$ . Here we use  $\Delta_A = \Delta_B = 0$ , and  $\eta/g = 0.7$ . (d) Fourier domain of population dynamics, in both cases the dashed lines are the data with cavity detuning ( $\Delta_c/g = 0.25$ ) and solid ones for  $\Delta_c = 0$ . The dynamical features and the frequency peaks remain largely unchanged with finite  $\Delta_c$ . In both cases  $g/\kappa = 0.1$ .

## V. STRONG-SYMMETRY EIGENSTATES FOR THE TWO-SPECIES MODEL

In this section, we expand on the discussion about strong symmetries that we outline in the *Symmetries and dynamical phases in the two-species model* section of the main text to further highlight the role of the tunable phase parameter.

We give a simple example to further understand the nature of the symmetry operator. With  $N_A = N_B = 1$ , the strong symmetry operator  $\mathbf{S}_\varphi^2$ , is trivially diagonalized into the eigenbasis

$$|T^\varphi\rangle = \{ |\downarrow\downarrow\rangle, (|\uparrow\downarrow\rangle + e^{-i\varphi} |\downarrow\uparrow\rangle)/\sqrt{2}, |\uparrow\uparrow\rangle \}, \quad |S^\varphi\rangle = (|\uparrow\downarrow\rangle - e^{-i\varphi} |\downarrow\uparrow\rangle)/\sqrt{2} \quad (\text{S57})$$

which, for  $\varphi = 0$  correspond to the usual triplet and singlet angular momentum eigenstates for a system of two qubits [60], see Fig. S3(a). Recall  $\varphi$  is a controllable optical phase associated with the complex Rabi frequencies driving the Raman transitions in the underlying multilevel atomic scheme (S12). Varying  $\varphi$ , we can see in the  $m_z = 0$  manifold there exists a continuous family of singlet states with orthogonal projection to the symmetric triplet state, see Fig. S3(b). The states with positive and negative magnetization  $m_z = \pm 1$  remain unchanged in this operation. Since the dynamics cannot mix distinct sectors, the weights of the initial state in the singlet and triplet manifolds dictate the accessible dynamical pathways and steady states.

However, the tunable phase  $\varphi$  directly shapes this sector decomposition by altering the physical content of the eigenstates themselves. Consider the initial superposition  $|+_x\rangle = (|\uparrow\downarrow\rangle + |\downarrow\uparrow\rangle)/\sqrt{2}$ . Its overlap with the phase-dependent singlet is

$$\langle S^\varphi | +_x \rangle = \frac{1 - e^{-i\varphi}}{2}. \quad (\text{S58})$$

For  $\varphi = 0$  this overlap vanishes and  $|+_x\rangle$  lies entirely in the symmetric manifold. Tuning  $\varphi$  to  $\pi$  yields  $|S^\pi\rangle = |+_x\rangle$ , so the same initial state becomes purely antisymmetric. Thus control of  $\varphi$  provides a simple mechanism to steer population between symmetric and antisymmetric sectors. Because the antisymmetric sector is often decoupled from collective decoherence channels, this phase-control can be exploited to protect entangled states from collective loss or dephasing.

We can directly expand these insights to larger spin ensembles. For a composite system of  $N = N_A + N_B \gg 1$  spin-1/2 particles, the Hilbert space decomposes into sectors of well-defined total spin  $S^2$ , as dictated by the rules of angular momentum addition [60]. These sectors range from  $S_{\min}^2 = |N_A - N_B|/2$  to the maximum  $S_{\max}^2 = |N_A + N_B|/2$ . The maximum sector corresponds to the fully permutationally invariant subspace spanned by Dicke states [62, 63]. Subspaces with lower  $S^2$  possess progressively less permutation symmetry, with the fully antisymmetric states at  $S^2 = S_{\min}^2$ , Fig. S3(c).

Crucially, the strong symmetry operator  $\mathbf{S}_\varphi^2$  continues to distinguish these sectors, and the phase  $\varphi$  controls the physical basis states within each. As in the two-spin case, varying  $\varphi$  coherently rotates the eigenbasis, thereby redistributing the overlap of a given initial state among the different symmetry sectors. This coherent redistribution of population directly influences the system's collective behavior

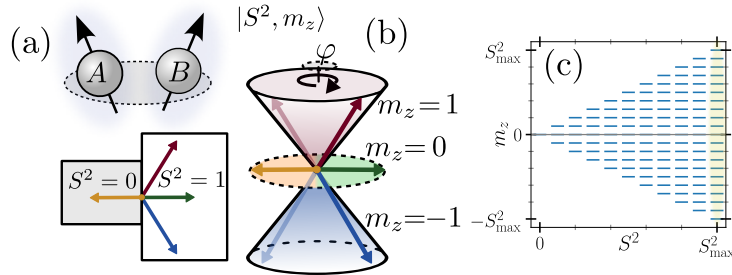


FIG. S3. **Total spin angular momentum eigenstates.** (a) For a generic two spin-1/2 system, the combined state decomposes into a symmetric triplet manifold,  $S^2 = 1$  and an antisymmetric singlet state,  $S^2 = 0$ . Within the  $m_z = 0$  subspace the phase  $\varphi$  can be seen as parametrizing rotations between the symmetric (green) and antisymmetric (orange) eigenstates (b). When generalizing to higher system sizes  $\gg 1$ , the Hilbert space decomposes into a family of permutation invariant states parametrized by  $S^2$  and  $m_z$  (c). For  $N_A = N_B$ , the rightmost ladder (shaded yellow) corresponds to the fully symmetric (Dicke) subspace,  $S^2 = N/2$ , and the fully antisymmetric subspace corresponds to the unique  $S^2 = 0 = m_z$  state.

because each spin sector is characterized by a distinct effective spin length  $S^2$ , which governs its degree of permutation symmetry and collective enhancement.

By varying  $\varphi$ , one can steer the initial state's overlap toward sectors with a lower effective spin  $S^2$ , thereby reducing the system's overall susceptibility to collective dissipation (since a fraction of the population is now within the antisymmetric subspace) while keeping the external driving rate unchanged. This mechanism effectively lowers the dynamical thresholds for many-body phases by adjusting  $\varphi$  alone, providing an effective and experimentally accessible control knob.

## VI. DECOHERENCE-FREE SUBSPACES AND THE EFFECT OF THE RELATIVE PHASE ON LIOUVILLIAN EIGENSPECTRA FOR THE TWO-SPECIES MODEL

In this section, we highlight the role of the spin detuning in inducing decoherence-free subspaces, and also the effect of relative phase on the eigenspectrum properties of the Liouvillian of the coupled spin-1/2 model.

Since  $\mathcal{L}$  is a non-hermitian matrix, it exhibits different left and right eigenmatrices; we denote these as  $\nu_\alpha$  and  $\mu_\alpha$ , respectively, defined by

$$\mathcal{L}[\nu_\alpha] = \lambda_\alpha \nu_\alpha, \quad \mu_\alpha(\mathcal{L}[\cdot]) = \lambda_\alpha \mu_\alpha(\cdot), \quad (\text{S59})$$

for eigenvalues  $\lambda_\alpha$  and chosen to satisfy the biorthogonality condition  $\text{Tr}(\mu_\alpha^\dagger \nu_\beta) = \delta_{\alpha\beta}$ .

With this spectral decomposition, the dynamical map  $e^{\mathcal{L}t}$  admits the standard expansion [61]

$$e^{\mathcal{L}t}[\cdot] = \sum_{\alpha} e^{\lambda_\alpha t} \nu_\alpha \text{Tr}(\mu_\alpha^\dagger \cdot), \quad (\text{S60})$$

where each factor  $e^{\lambda_\alpha t}$  dictates the decay and oscillations of its associated eigenmode  $\nu_\alpha$ , its real part setting the decay rate and its imaginary part the frequency. This decomposition allows us to isolate and examine specific eigenmodes. The full spectrum of  $\mathcal{L}$  for the spin-1/2 system for  $N_A = N_B = N/2 = 3$  is shown in Fig. S4 (a)–(d).

For zero spin detuning, the spectrum lies entirely on the negative real axis, so that all oscillations become damped for finite system sizes. Extending the system to the thermodynamic limit ( $N \rightarrow \infty$ ) allows these oscillations to persist in the form of nonstationary states (NSS) when driving rate is appropriately increased (see Fig 2 in the main text and its discussion).

When an equal and finite detuning  $\Delta$  is introduced, a pair of purely imaginary eigenvalues,  $\lambda_{\pm} = \pm i\Delta$ , appears even for finite  $N$ . The associated eigenmodes are unaffected by the dissipators and therefore form a decoherence-free subspace (DFS). Importantly, while the eigenvalues  $\lambda_{\pm}$  depend on  $\Delta$  and the associated eigenvectors  $\nu_{\pm}$  depend on the relative phase  $\varphi$ , physical contributions to the dynamics are given by the product  $e^{\lambda_{\pm} t} \nu_{\pm} = e^{\pm i\Delta t} \nu_{\pm}(\varphi)$ . The contribution of this pair to the time-evolved density matrix reads

$$\rho_{\pm}(t) = e^{\lambda_{\pm} t} c_{\pm}(\varphi) \nu_{\pm}(\varphi) = e^{\pm i\Delta t} c_{\pm}(\varphi) \nu_{\pm}(\varphi), \quad (\text{S61})$$

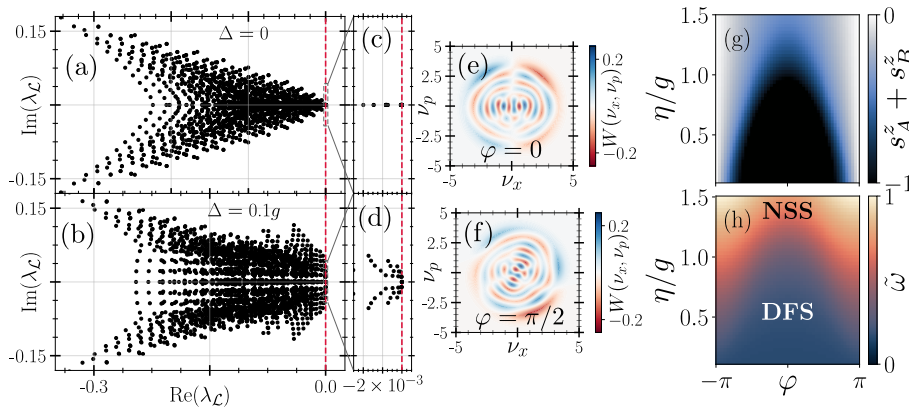


FIG. S4. **Role of spin detuning and relative phase on spin-1/2 Liouvillian spectrum.** Liouvillian eigenvalue ( $\lambda_{\mathcal{L}}$ ) spectrum for  $N_A = N_B = 3$  for equal spin detunings  $\Delta_A = \Delta_B \equiv \Delta$ , for  $\Delta = 0$  (a) and  $\Delta = 0.1g$  (b). Zoomed in regions close to the  $\text{Re}(\lambda_{\mathcal{L}}) = 0$  line highlight the nature of the long time behaviour. Besides the unique  $\text{Re}(\lambda_{\mathcal{L}}) = \text{Im}(\lambda_{\mathcal{L}}) = 0$  steady state, we find purely decaying modes ( $\text{Re}(\lambda_{\mathcal{L}}) < 0$ ) in (c) and the existence of purely imaginary eigenvalues  $\text{Im}(\lambda_{\mathcal{L}}) = \pm\Delta$  in (d), indicators of a decoherence-free subspace. The phase  $\varphi$  does not contribute to the eigenvalue spectrum, but it can be used to rotate the eigenvectors of the Liouvillian. In (e)-(f) we plot the Wigner function of the eigenvector  $|\nu_+\rangle$  for  $N_A = N_B = 1$ , corresponding to the  $\lambda_+ = i\Delta$  mode, for two choices of  $\varphi$ . Other parameters used  $\eta/\kappa = 0.025$ ,  $\Delta_c = 0$  and  $g/\kappa = 0.1$ . In analogy to Fig. 2 in the main text, we map out the resulting mean field phase diagram for nonzero detunings  $\Delta = 0.1g$ , showing both the total magnetization (g) and the dominant normalized frequency  $\tilde{\omega}_A$  (h) used to discern between a Decoherence-Free Subspace (DFS) and Nonstationary States (NSS). The DFS is confirmed by the presence of oscillatory regions of constant frequency in the phase diagram ( $\tilde{\omega}_A \neq 0$ ) regardless of driving strength, as the driving rate is increased we recover the nonstationary states of the kind outlined in the main text.

where

$$c_{\pm}(\varphi) = \text{Tr}(\mu_{\pm}(\varphi)^{\dagger} \rho(0)). \quad (\text{S62})$$

Consequently, the contribution of the decoherence-free pair to the expectation value of any observable  $O$  is

$$\langle O \rangle_{\pm}(t) = e^{\pm i\Delta t} A_O(\varphi), \quad \text{for} \quad A_O(\varphi) \equiv c_{\pm}(\varphi) \text{Tr}(O \nu_{\pm}(\varphi)). \quad (\text{S63})$$

Two immediate and useful observations follow. First,  $\Delta$  fixes the oscillation frequency. Second, the amplitude  $A_O(\varphi)$  depends explicitly on  $\varphi$  through the left and right eigenmodes: changing  $\varphi$  rotates the decoherence-free eigenvectors in Liouville-space and thereby modifies the overlaps

$$\text{Tr}(\mu_{\pm}(\varphi)^{\dagger} \rho(0)) \quad \text{and} \quad \text{Tr}(O \nu_{\pm}(\varphi)).$$

As a result, for fixed  $\rho(0)$  one can continuously tune  $A_O(\varphi)$  by varying  $\varphi$ , and in particular make it vanish or become nonzero. In physical terms,  $\varphi$  acts as a control knob that rotates the eigenbasis and thus enables or suppresses oscillatory behaviour in parameter or initial-state regimes where it was otherwise absent for other values of  $\varphi$ . This mode rotation is directly visible in the Wigner function plots of  $\nu_+(\varphi)$  (Fig. S4(e)-(f)). We note this rotation is not unique to the decoherence-free subspace as indeed all eigenvectors are phase dependent,  $\nu_{\alpha}(\varphi)$ .

In analogy to Fig. 2 in the main text, panels (g)-(h) map the mean-field phase diagram in the thermodynamic limit  $N \rightarrow \infty$  for nonzero detuning. Panel (g) shows the total magnetization  $s_A^z + s_B^z$  and (h) the dominant normalized oscillation frequency  $\tilde{\omega}$ , which we use to discriminate between the DFS and NSS. The DFS is identified by extended  $\tilde{\omega}_A = \text{const.} \neq 0$  regions across the driving axis  $\eta/g$ , indicating robust oscillations whose frequency is fixed by  $\Delta$ . Increasing the driving amplitude  $\eta/g$  drives the system deeper into the nonstationary regimes discussed in the main text. Importantly, DFS regions occur at negative total magnetization, showing that the decoherence-free oscillatory behavior is not restricted to the usual  $s^z \approx 0$  order parameter sector for NSS.

## VII. THREE-LEVEL SYSTEM DYNAMICS

In this section, we present the algebraic structure of the three-level system, along with the equations of motion that define its dynamics in the Gell-Mann basis.

Since the atomic level scheme now shares a common level  $|0\rangle$  (Fig. S1(b)), we cannot write it in terms of Pauli-spin matrices following  $\mathfrak{su}(2)$  algebra. However we can describe the system in terms of the Gell-Mann matrices defined as follows:

$$\begin{aligned}\hat{\lambda}_1 &= \frac{1}{2} \begin{bmatrix} 0 & 1 & 0 \\ 1 & 0 & 0 \\ 0 & 0 & 0 \end{bmatrix}, & \hat{\lambda}_2 &= \frac{1}{2} \begin{bmatrix} 0 & -i & 0 \\ i & 0 & 0 \\ 0 & 0 & 0 \end{bmatrix}, & \hat{\lambda}_3 &= \frac{1}{2} \begin{bmatrix} 1 & 0 & 0 \\ 0 & -1 & 0 \\ 0 & 0 & 0 \end{bmatrix}, \\ \hat{\lambda}_4 &= \frac{1}{2} \begin{bmatrix} 0 & 0 & 1 \\ 0 & 0 & 0 \\ 1 & 0 & 0 \end{bmatrix}, & \hat{\lambda}_5 &= \frac{1}{2} \begin{bmatrix} 0 & 0 & -i \\ 0 & 0 & 0 \\ i & 0 & 0 \end{bmatrix}, & \hat{\lambda}_6 &= \frac{1}{2} \begin{bmatrix} 0 & 0 & 0 \\ 0 & 0 & 1 \\ 0 & 1 & 0 \end{bmatrix}, \\ \hat{\lambda}_7 &= \frac{1}{2} \begin{bmatrix} 0 & 0 & 0 \\ 0 & 0 & -i \\ 0 & i & 0 \end{bmatrix}, & \hat{\lambda}_8 &= \frac{1}{2\sqrt{3}} \begin{bmatrix} 1 & 0 & 0 \\ 0 & 1 & 0 \\ 0 & 0 & -2 \end{bmatrix}.\end{aligned}\tag{S64}$$

These matrices are traceless and Hermitian, making them generators of the SU(3) group. The Gell-Mann matrices satisfy the following commutation relations:

$$[\hat{\lambda}_a, \hat{\lambda}_b] = if_{abc}\hat{\lambda}_c\tag{S65}$$

where  $f_{abc}$  are the structure constants of the  $\mathfrak{su}(3)$  algebra, which are completely antisymmetric. Important non-zero values are:

$$f_{123} = 1, \quad f_{147} = f_{246} = f_{257} = f_{345} = \frac{1}{2}, \quad f_{156} = f_{367} = -\frac{1}{2}, \quad f_{458} = f_{678} = \frac{\sqrt{3}}{2}.\tag{S66}$$

The anticommutation relations are given by:

$$\{\hat{\lambda}_a, \hat{\lambda}_b\} = \frac{4}{3}\delta_{ab}I + 2d_{abc}\hat{\lambda}_c\tag{S67}$$

where  $d_{abc}$  are the symmetric structure constants.

The equations of motion for each of the Gell-Mann matrices can be evaluated using their commutative properties, where the structure will be split into the  $0 \leftrightarrow A$  sector (generators  $\hat{\lambda}_1$  and  $\hat{\lambda}_2$ ), the  $A \leftrightarrow B$  sector (generators  $\hat{\lambda}_4$  and  $\hat{\lambda}_5$ ) and the  $0 \leftrightarrow B$  sector (generators  $\hat{\lambda}_6$  and  $\hat{\lambda}_7$ ), with *inter-sector* couplings mediated by cavity-allowed interactions.

$$\begin{aligned}\dot{\hat{\lambda}}_1 &= -\Delta_A \hat{\lambda}_2 + ig \left[ \hat{\lambda}_3 (\hat{a} - \hat{a}^\dagger) + \frac{e^{-i\varphi} \hat{a}^\dagger}{2} (-i\hat{\lambda}_5 + \hat{\lambda}_4) + \frac{e^{i\varphi} \hat{a}}{2} (-i\hat{\lambda}_5 - \hat{\lambda}_4) \right] \\ \dot{\hat{\lambda}}_2 &= \Delta_A \hat{\lambda}_1 + ig \left[ i\hat{\lambda}_3 (\hat{a}^\dagger + \hat{a}) + \frac{e^{-i\varphi} \hat{a}^\dagger}{2} (i\hat{\lambda}_4 + \hat{\lambda}_5) + \frac{e^{i\varphi} \hat{a}}{2} (i\hat{\lambda}_4 - \hat{\lambda}_5) \right] \\ \dot{\hat{\lambda}}_3 &= ig \left[ -i\hat{\lambda}_2 (\hat{a}^\dagger + \hat{a}) + \hat{\lambda}_1 (\hat{a}^\dagger - \hat{a}) + \frac{e^{-i\varphi} \hat{a}^\dagger}{2} (i\hat{\lambda}_7 - \hat{\lambda}_6) + \frac{e^{i\varphi} \hat{a}}{2} (i\hat{\lambda}_7 + \hat{\lambda}_6) \right] \\ \dot{\hat{\lambda}}_4 &= -(\Delta_A - \Delta_B) \hat{\lambda}_5 + ig \left[ \frac{\hat{a}^\dagger}{2} (i\hat{\lambda}_7 + \hat{\lambda}_6) + \frac{\hat{a}}{2} (i\hat{\lambda}_7 - \hat{\lambda}_6) + \frac{\hat{a}^\dagger e^{-i\varphi}}{2} (-i\hat{\lambda}_2 - \hat{\lambda}_1) + \frac{\hat{a} e^{i\varphi}}{2} (-i\hat{\lambda}_2 + \hat{\lambda}_1) \right] \\ \dot{\hat{\lambda}}_5 &= (\Delta_A - \Delta_B) \hat{\lambda}_4 + ig \left[ \frac{\hat{a}^\dagger}{2} (-i\hat{\lambda}_6 + \hat{\lambda}_7) + \frac{\hat{a}}{2} (-i\hat{\lambda}_6 - \hat{\lambda}_7) + \frac{\hat{a}^\dagger e^{-i\varphi}}{2} (i\hat{\lambda}_1 - \hat{\lambda}_2) + \frac{\hat{a} e^{i\varphi}}{2} (i\hat{\lambda}_1 + \hat{\lambda}_2) \right] \\ \dot{\hat{\lambda}}_6 &= \Delta_B \hat{\lambda}_7 + ig \left[ \frac{\hat{a}^\dagger}{2} (i\hat{\lambda}_5 - \hat{\lambda}_4) + \frac{\hat{a}}{2} (i\hat{\lambda}_5 + \hat{\lambda}_4) + \frac{1}{2} (e^{i\varphi} \hat{a} - e^{-i\varphi} \hat{a}^\dagger) (\sqrt{3}\hat{\lambda}_8 - \hat{\lambda}_3) \right] \\ \dot{\hat{\lambda}}_7 &= -\Delta_B \hat{\lambda}_6 + ig \left[ \frac{\hat{a}^\dagger}{2} (-i\hat{\lambda}_4 - \hat{\lambda}_5) + \frac{\hat{a}}{2} (-i\hat{\lambda}_4 + \hat{\lambda}_5) + \frac{1}{2} (e^{i\varphi} \hat{a} + e^{-i\varphi} \hat{a}^\dagger) (i\sqrt{3}\hat{\lambda}_8 - i\hat{\lambda}_3) \right] \\ \dot{\hat{\lambda}}_8 &= -i\frac{\sqrt{3}}{2}g \left[ \hat{a}^\dagger e^{-i\varphi} (i\hat{\lambda}_7 - \hat{\lambda}_6) + \hat{a} e^{i\varphi} (i\hat{\lambda}_7 + \hat{\lambda}_6) \right] \\ \dot{a} &= \left( i\Delta - \frac{\kappa}{2} \right) a - ig \left[ (\hat{\lambda}_1 - i\hat{\lambda}_2) + e^{-i\varphi} (\hat{\lambda}_6 - i\hat{\lambda}_7) \right] + \eta\end{aligned}\tag{S68}$$

Note  $\hat{\lambda}_3$  and  $\hat{\lambda}_8$  are sufficient to fully define the population in level  $i$  via  $\hat{N}_i$ , with

$$\begin{aligned}\hat{N}_A &= \frac{\hat{I}}{3} + \hat{\lambda}_3 + \frac{1}{\sqrt{3}}\hat{\lambda}_8, \\ \hat{N}_0 &= \frac{\hat{I}}{3} - \hat{\lambda}_3 + \frac{1}{\sqrt{3}}\hat{\lambda}_8, \\ \hat{N}_B &= \frac{\hat{I}}{3} - \frac{2}{\sqrt{3}}\hat{\lambda}_8.\end{aligned}\tag{S69}$$

*SU(3) analogue of spin-length conservation-*

For the collective spin system defined by SU(2) algebra, the conserved quantity is the quadratic Casimir

$$\langle \mathbf{S}^2 \rangle = \langle S_x^2 + S_y^2 + S_z^2 \rangle = s(s+1),\tag{S70}$$

which is constant under any Hamiltonian built from  $S_x, S_y, S_z$ .

For an SU(3) system defined by the Gell-Mann matrices  $\{\hat{\lambda}_1, \dots, \hat{\lambda}_8\}$ , the direct analogue is the quadratic Casimir operator

$$\hat{C}_2 = \sum_{a=1}^8 \hat{\lambda}_a \hat{\lambda}_a,\tag{S71}$$

so that for any pure state in the fundamental representation,  $\langle \hat{C}_2 \rangle = \frac{1}{3}$ .

Additionally, because  $\mathfrak{su}(3)$  is a rank-2 algebra, there exists a cubic Casimir operator

$$\hat{C}_3 = \sum_{a,b,c} d_{abc} \hat{\lambda}_a \hat{\lambda}_b \hat{\lambda}_c,\tag{S72}$$

where  $d_{abc} = \frac{1}{4} \text{Tr}(\{\hat{\lambda}_a, \hat{\lambda}_b\} \hat{\lambda}_c)$  are the completely symmetric structure constants of  $\mathfrak{su}(3)$ . This operator also commutes with all generators, and

$$\langle \hat{C}_3 \rangle = \frac{10}{9 \cdot 2^3}$$

is likewise conserved.

## VIII. DECOHERENCE-FREE SUBSPACES FOR COLLECTIVE THREE-LEVEL SYSTEM

Similar to the two-species spin-1/2 system, we focus our attention to the rich dynamical features emerging from the effects of finite detuning  $\Delta_A = \Delta_B \neq 0$  for the collective three-level system. In this case, we can find two other unique non-stationary phases when the detunings are nonzero. Accordingly, we concentrate on finite-size effects and on how the Liouvillian spectral properties depend on detunings  $\Delta_A, \Delta_B$ . We stress that all features described below are independent of driving strength  $\eta$  and, as such, different from the nonstationary state oscillations described in the main text in the  $\Delta = 0$  case.

### Decoherence free subspace for $\Delta_A = \Delta_B \equiv \Delta$

As discussed previously in the spin-1/2 scenario, a finite detuning  $\Delta$  introduces an energy splitting between the ground and excited states. This coherent term generates unitary evolution within the bright manifold in the form of a DFS. This is again marked by Liouvillian eigenmodes with purely imaginary eigenvalues  $\text{Im}(\lambda_{\mathcal{L}}) = \pm i\Delta$ . These correspond to oscillations in the single particle picture between the  $|0\rangle_j$  and  $|+\rangle_j$  eigenstates at frequency  $\Delta$ . The emergence of these modes is clearly visible at finite sizes, see Fig. S5(a) which is evaluated for  $N = 2$  atoms.

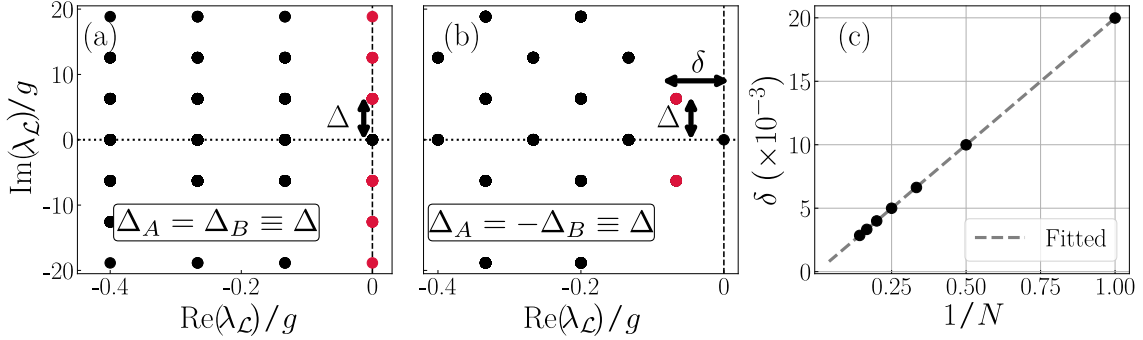


FIG. S5. **Finite and emergent DFS.** Parameter-dependent DFS (a) and emergent DFS (b). Closing of the Liouvillian gap at increasing system sizes for  $N \in \{1, 2, \dots, 7\}$  (c). In the above we have chosen  $\eta/\kappa = 0.025$ ,  $\Delta/\kappa = 0.2\pi$  and  $g/\kappa = 0.1$ . The red dots represent the points with the smallest real gap.

### Emergent decoherence free subspace for $\Delta_A = -\Delta_B \equiv \Delta$

In this case, the strong symmetry generator we found in the main text no longer applies, as the detuning pattern creates a new symmetry structure. The effective Hamiltonian now contains terms  $\hbar\Delta(\hat{\Lambda}_A^\dagger \hat{\Lambda}_A - \hat{\Lambda}_B^\dagger \hat{\Lambda}_B)$  that distinguish between the  $A$  and  $B$  excited states. At the single particle level, this leads to the formation of dressed states  $|\pm\rangle_j$  with energy splitting  $2\Delta$ . The jump operator  $\hat{\Lambda}_\varphi$  couples predominantly to one combination of these dressed states, while the orthogonal combination becomes increasingly protected as system size grows.

The gapped real part observed for finite system sizes arises from weak residual coupling between the protected manifold and the dissipative sector, causing slow decay  $\delta$  at rate  $\sim \mathcal{O}(1/N)$ . As  $N \rightarrow \infty$ , this coupling vanishes, and the real part gap closes, revealing a true decoherence-free subspace analogous to the  $\Delta_A = \Delta_B$  case. Meanwhile, the imaginary gap of size  $\Delta$  persists because it stems from the inherent energy splitting between the dressed states, which remains finite regardless of system size. This explains why the imaginary spectrum maintains a  $\Delta$ -sized gap, while the real gap exhibits finite-size scaling to zero. Both of these features are clearly visible from the Liouvillian spectrum for increasing system sizes, Fig. S5(b)-(c).